The University of Alabama in Huntsville

FINAL Report

CHARACTERISTICS AND PERFORMANCE OF THE VARIABLE POLARITY PLASMA ARC WELDING PROCESS USED IN THE SPACE SHUTTLE EXTERNAL TANK

NASA CONTRACT: NAS8-36955/

Delivery Order No. 37

Prepared by

R. J. Hung, C. C. Lee, and J. W. Liu

The University of Alabama in Huntsville

Huntsville, Alabama 35899

July 1990

ABSTRACT

Significant advantages of Variable Polarity Plasma Arc (VPPA) welding process include faster welding, fewer repairs, less joint preparation, reduced weldment distortion , and absence of porosity. Flow profiles and power distribution of argon plasma gas as a working fluid to produce plasma arc jet in the VPPA welding process has been analyzed. Major loss of heat transfer for flow through nozzle is convective heat transfer; for flow of plasma jet between outlet of nozzle to workpiece is radiative heat transfer; and for flow through keyhole of workpiece is convective heat transfer. Majority of power absorbed by the keyhole of workpiece is used for melting the solid metal workpiece to become molten metalic puddle. Crown and roo widths, and crown and root heights can be predicted from the prese study. Present study provides an algorithm for promoting autom control of flow parameters and the dimensions of final produ welding specification to be used for the VPPA welding system or at the NASA Marshall Space Flight Center (NASA/MSFC).

I. Introduction

The plasma arc is a concentrated energy source commonly used in welding and cutting processes. It is composed of a partially ionized gas stream produced by forcing an inert gas to flow through an electric field and emerge from a constricting nozzle. With its high energy density and velocity, the plasma arc, when impinging on the workpiece, can create a hole in the molten liquid pool and penetrate through it. Depending on the operating parameters employed, this hole may either become self-healing or remain open as the arc transverses along the workpiece. A "keyhole" welding process occurs in the self-healing case, in which the molten metal in front of the arc flows around the arc column and resolidifies behind the arc. On the other hand, a cutting operation is achieved if the hole remains open (O'Brien, 1968).

In the plasma welding process fusion is produced by the heat of a constricted arc. It is essentially an extension of gas tungsten-arc welding (GTAW), but much higher energy density in the arc and much higher gas velocity and momentum are produced by constraining the arc to flow through a nozzle. One important characteristic of plasma arc welding is the ability of the process to produce deep penetration welds by forming a "keyhole" in the workpiece. This is distinct from the essentially "surface melting" produced by the GTAW process (which can not normally penetrate to a depth equal to the width of a weld pool). The plasma arc produces a "keyhole" in the weld pool by pressure of the gas flow. When the process operates correctly, the metal which is melted in front of the advancing "keyhole" flows round to the rear where it solidifies to form the weld bead.

In 1955 Linde Air Products introduced a plasma arc torch for metal cutting applications, and by 1965 Linde had developed an automatic plasma arc welding facility for Westinghouse Electric Corporation to fabricate 120 in. diameter, 3/8 in. thick D6AC steel rocket motor case for the Titan III-C booster assembly (Miller and Filipski, 1966; Privoznik and Miller, 1966). The plasma arc welding process was reported to have halved the welding time required. Then in 1965 Thermal Dynamics Corporation reported the use of direct current reversed polarity (workpiece negative) plasma arc to join 1/4 in. thick aluminum plate (Cooper el al., 1965). At the end of the decade of the 1960's, Van Cleave at the Boeing Company began his efforts to combine the plasma arc process with a variable polarity feature wherein the electrode polarity was periodically reversed. Alternating electrode potential for aluminum welding had been investigated as early as 1947 (Herbst, 1947). Difficulties with welding power supplies in this application were evident early-on and when variable polarity plasma arc (VPPA) welding was used in the U.S. Army Roland Missile Production Program, development problems such as arc pressure pulsation were noted (Nunes et al., 1981; 1983). As a result of Van Cleave's promising work at Boeing, a VPPA research and development project was initiated in 1978 at the NASA Marshall Space Flight Center, intended to determine the potential for replacing the GTAW system used in the fabrication of the Space Shuttle External Tank (ET). Certain improvements were made to the original equipment and process, VPPA welding finally exceeded the expectations (Nunes et al., 1984a; 1984b).

The Space Shuttle ET is the largest known "drop tank" carrying 140,000 gallons of liquid oxygen and 380,000 gallons of liquid hydrogen, with the dimensions 28.6 feet in diameter and 154 feet in length. From the initiation of ET production, the conventional GTAW system operating in the direct current electrode negative mode was used. In fabricating the large Saturn lunar rocket first stage with the GTAW system, weld porosity and inclusions had been ever-present problems throughout the entire program, and the decision to use 100% radiographic inspection was made at the outset. Weld porosity and inclusions had to be systematically ground out and weld repaired which made the replacement of GTAW system by VPPA welding process advantageous.

Significant advantages of the VPPA process include faster welding, fewer repairs, less joint preparation, reduced weldment distortion, and absence of porosity.

In this study, flow profile and power distribution of argon arc plasma through the entire VPPA welding process has been analyzed. This study includes the system analysis of following sections: (1) Pilot arc and main arc power distribution and the total power input of the VPPA welding system; (2) Plasma arc power loss through nozzle which accelerate arc plasma gas and transform potential energy to kinetic energy which form the plasma jet at the outlet of nozzle; (3) Radiative and convective heat loss of plasma jet column from the outlet of nozzle to the plasma jet approaching workpiece; (4) Flow criteria of partial penetration and full penetration plasma arc jet through workpiece; and (5) Determination of crown width, crown

height, root width and root height for horizontal and vertical welding.

II. Variable Polarity Electric Power System

The significant current carriers in a welding arc are electrons and positive ions. Electrons carry the bulk of the current, moving rapidly from negative cathode to positive anode. The positive ions drift more slowly through the interelectrode space. The differential drift rate results in an unsymmetrical heating at the ends of the welding arc in a fixed polarity arrangement. The cathode receives less heat and the anode more heat. The "straight polarity" mode of operation entails a negative electrode (cathode) and a positive workpiece (anode). Where the primary object of the weld process is to deliver the maximum heat to the workpiece with minimum deterioration of the electrode, straight polarity is used.

"Reverse polarity", which is positive electrode and negative workpiece, has the advantage that the workpiece is subjucted to a cleaning process (cathode cleaning) by the impingement of heavy (compared to electron) positive ions on the workpiece surface. In the case of plasma arc welding reverse polarity action appears to condition the surface of the aluminum alloy so that the molten metal flows easily and controllably under the arc. It is conjectured that this fluid control is accomplished through breaking up of surface oxide films. Cutoff of reverse polarity during VPPA welding transforms a weld metal flow which closes smoothly and soundly behind the keyhold to an irregular, intermittent, globular flow leaving a rough, lumpy bead sunken below the parent metal surface and protruding

jaggedly from the root of the weld. But continuous reverse polarity is not necessary to provide adequate cathodic cleaning action.

The variable polarity square-wave with unequal straight and reverse polarity time intervals offered a combination of the high heating capability of straight polarity with the cleaning feature of reverse polarity. Adequate cleaning is obtained by incorporating a relatively short (one tenth to one fifth the duration of the straight polarity current) pulse of reverse polarity current into welding current waveform.

Figure 1 show the VPPA electric power system. During the straight polarity mode of operation, it employs a negative electrode (cathode) and a positive workpiece (anode), while it employs a positive electrode and a negative workpiece during the reverse polarity mode of operation. At left of Figure 1 illsustrates the straight polarity mode, and the reverse polarity mode is shown on the right-hand-side of the figure.

Let ϕ_1, ϕ_2, and ϕ_3 denote the workfunctions for tungsten electrode, nozzle and workpiece, respectively. V_a and V_c are anode and cathode drops, respectively; while $(\epsilon_+)_1$ and $(\epsilon_-)_1$ are the pilot arc voltages in straight polarity and reverse polarity, respectively. u shows the voltage drop per unit length in the arc column. One can derive the pilot arc voltages in the straight polarity and reverse polarity as follows:

(A) Straight Polarity

$$U_E = U_F - V_a - \phi_3 = -V_a - \phi_3$$

$$U_C = U_E - u(L_1 + d_3) = -V_a - \phi_3 - u(L_1 + d_3)$$

$$U_B = U_E - u(d_3 + d_2) = -V_a - \phi_3 - u(d_3 + d_2)$$

$$U_D = U_C + V_a + \phi_2 = -V_a - \phi_3 - u(L_1 + d_3) + V_a + \phi_2$$

$$= \phi_2 - \phi_3 - u(L_1 + d_3)$$

$$U_A = U_B - V_C + \phi_1 = -V_a - \phi_3 - u(d_3 + d_2) - V_C + \phi_1$$

$$(\epsilon_+)_1 = U_D - U_A = \phi_2 - \phi_3 - u(L_1 + d_3) + V_a + \phi_3$$

$$+ u(d_3 + d_2) + V_C - \phi_1$$

$$= \phi_2 - \phi_1 + V_a + V_C + u(d_2 - L_1)$$

(B) Reverse Polarity

Voltage difference between point E and E', shown in Figure 1 is affected by the cathode section of workpiece. As the aluminum is not an ideal thermionic material, the voltage drop of workpiece could be greater than that of the ideal thermionic metal, such as tungsten. Assuming $U_{EE'} = \alpha$, pilot arc power supply in reverse polarity can be evaluated as follows:

$$U_E' = U_F' + V_C - \phi_3 = V_C - \phi_3$$

$$U_C' = U_E' + \alpha + u(d_3 + L_1) = V_C - \phi_3 + u(d_3 + L_1) + \alpha$$

$$U_B' = U_E' + \alpha + u(d_3 + d_2) = V_C - \phi_3 + u(d_3 + d_2) + \alpha$$

$$U_D' = U_C' + V_a + \phi_2 = V_C - \phi_3 + u(d_3 + L_1) + \alpha + V_a + \phi_2$$

$$U_A' = U_B' + V_a + \phi_1 = V_C - \phi_3 + u(d_3 + d_2) + \alpha + V_a + \phi_1$$

$$(\epsilon_-)_1 = U_D' - U_A'$$

$$= U_C - \phi_3 + u(d_3 + L_1) + \alpha + V_a + \phi_2 - V_C + \phi_3$$

$$- u(d_3 + d_2) - \alpha - V_a - \phi_1$$

$$= \phi_2 - \phi_1 - u(d_2 - L_1)$$

Reasonable values obtained from the literature and from limited experimentation at NASA Marshall Space Flight Center yield the following values specified: $\phi_1 = 2.6V$, $\phi_2 = 4.5V$, $\phi_3 = 4.2V$, $V_C =$

6.5V, V_a = 7.0V, u= 35.5V/in. Typical geometric parameters are: L_1 = 0.133 in, L_2 = 0.375 in, d_2 = 0.178 in, and d_3 = 0.22 in. We can calculate the pilot arc voltages in the straight polarity and the reverse polarity as follows:

$$(\epsilon_+)_1 = \phi_2 - \phi_1 + V_a + V_c + u(d_2 - L_1)$$
$$= 4.5 - 2.6 + 7.0 + 6.5 + 35.5(0.178 - 0.133)$$
$$= 17 \text{ V}$$

$$(\epsilon_-)_1 = \phi_2 - \phi_1 - u(d_2 - L_1)$$
$$= 4.5 - 2.6 - 35.5(0.178 - 0.133)$$
$$= 0.3 \text{ V}$$

III. Total Power Input of the VPPA Welding System

The pilot arc current, superimposed upon the main arc current between the electrode and the plasma nozzle, is supplied by a seperate power supply located in the plasma control console. The pilot arc polarity does not alternate. The nozzle is held positive with respect to the electrode so that the electron flow is always away from the electrode toward the nozzle. The main arc is started by application of high frequency alternating voltage between the electrode and the plasma nozzle so as to first establish the pilot arc from which the main arc proceeds. The high frequency current is controlled by the plasma control console, but is generated by the spark gap oscillator located in the hot block.

The total electric power input of VPPA welding system includes the pilot arc between electrode and nozzle, and also the main power arc between electrode and workpiece during the straight polarity and the

reverse polarity modes. Following nomenclatures are given:

I_1 = pilot arc current

I_3 = main arc current

ϵ_1 = pilot arc voltage

ϵ_3 = main arc voltage

$(I_+)_3$ = main arc current in straight polarity

$(I_-)_3$ = main arc current in reverse polarity

t_+ = time period of straight polarity

t_- = time period of reverse polarity

The total electric power input of the VPPA welding system is given in the expression

$$P = I_1 \epsilon_1 + I_3 \epsilon_3$$

$$= I_1 \frac{(\epsilon_+)_1 t_+ + (\epsilon_-)_1 t_-}{t_+ + t_-} + \frac{(I_+)_3 (\epsilon_+)_3 t_+ + (I_-)_3 (\epsilon_-)_3 t_-}{t_+ + t_-}$$

Figure 2 shows the power input system and the dimension of the geometry. In the present VPPA welding system operated in the NASA/MSFC, time periods for the straight polarity and the reverse polarity are 19 sec and 4 sec, respcectively. Pilot arc currents for both straight and reverse polarities are 25 amp; while main arc currents for straight and reverse polarities are 195 and 200 amp, respectively. The pilot arc voltages for the straight and the reverse polarities are 17 and 0.3 V, respectively; while the main arc voltages for the straight and the reverse polarities are 32.5 and 40 V, respectively. Thus, we can calculate the total power input of the VPPA welding system operated in the NASA/MSFC as follows:

$$P = (25)\ \frac{(17)\ (19) + (0.3)\ (4)}{(19) + (4)}$$

$$+\ \frac{(195)(32.5)(19) + (200)(40)(4)}{(19) + (4)}$$

$$= 352.5 + 6626.63 = 6979.13\ W$$

The volumetric flow rate of argon gas to be used for plasma arc jet stream is regulated. In the present VPPA welding system operated in the NASA/MSFC, volumetric argon gas flow rate is 7.5 ft^3/hr at 25^0C. It can be converted to SI unit as follows:

$$\dot{Q} = (7.5\ ft^3/hr)\ (1/3600\ hr/s)\ (1/35.3147\ m^3/ft^3)\ \cdot$$

$$(10^6\ cm^3/m^3)$$

$$= 58.99\ cm^3/s$$

Argon gas density at 1 atmospheric pressure and 25^0C can be computed from the equation of state

$$p = \rho \frac{R}{M} T$$

where p denotes pressure; ρ, the density; R ($=82.05\ cm^3 \cdot atm/mole \cdot {}^0K$), the universal gas constant; M, the molecular weight (39.948 g/mole for argon gas); and T, the temperature. The argon gas density at 1 atmospheric pressure and the temperature of 25^0C can be computed as

$$(1\ atm) = \rho\ \frac{(82.05\ cm^3 \cdot\ atm/mole \cdot\ {}^0K)}{(39.948\ g/mole)}\ (298^0K)$$

which leads

$$\rho = 1.6249 \times 10^{-3}\ g/cm$$

Mass flow rate of argon gas, thus, can be obtained as

$$\dot{m} = \rho\dot{Q} = (1.6249 \times 10^{-3}\ g/cm^3)\ (58.99\ cm^3/s)$$

$$= 9.585 \times 10^{-2}\ g/s$$

Shielding gas is needed for the isolation of welding system from the surrounding environment, and for the cooling of workpiece from the high temperature injection of plasma arc. Shielding gas is an essential factor in achieving quality welds in any gas shielded arc welding process. The problem of impurities, when manifest, is normally resolved by eliminating the source of the contamination. However, if the gas supply itself is contaminated serious schedule interruptions can result, particularly where large manifolded gas distribution systems, are employed.

Gas contamination affects VPPA welding in several ways. Inside the torch, oxygen from water vapor decomposed in the arc can produce a visible oxide film stain on the tungsten electrode. The plasma jet may sputter and exhibit a green coloration from copper eroded from the nozzle under erratic flow conditions. The weld itself may exhibit a pocked-looking surface, presumed to be fine porosity due to hydrogen gas from decomposed water vapor. Under more severe conditions, the torch may leave behind it a train of irregularities and holes in the weld bead.

IV. Plasma Arc Power Loss Through Nozzle

Plasma arc power distribution in the whole variable polarity plasma arc welding system can be divided into the following four parts for the convenience of discussion: (1) plasma arc power before entering the nozzle (P_a); (2) plasma arc power after extracting from

the nozzle (P_b); (3) plasma arc power before entering the keyhole of workpiece (P_c); and (4) plasma arc power at the outlet end of the keyhole of workpiece (P_d). Figure 3 shows the plasma arc power distribution in the whole VPPA welding system.

In this section, plasma arc power loss through the nozzle will be discussed. Figure 4 shows the electric current and electric voltage drop distribution of the VPPA welding system. In addition to the nomenclatures given in Section III, there are some more terms, shown in Figure 4, are given as follows:

$\Delta\epsilon_+$ = voltage drop of electrode in straight polarity

$\Delta\epsilon_-$ = voltage drop of electrode in reverse polarity

ϵ_+' = voltage drop of nozzle in straight polarity

ϵ_-' = voltage drop of nozzle in reverse polarity

Estimation of plasma arc power distribution is based on the linear power distribution assumption of argon plasma gases between the point of entering the nozzle and the point of entering the keyhole of workpiece. Plasma arc power before entering the nozzle can be computed from the following equation:

$$P_a = I_1 \frac{(\Delta\epsilon_+)_1 t_+ + (\Delta\epsilon_-)_1 t_-}{t_+ + t_-} + \frac{(I_+)_3(\Delta\epsilon_+)_3 t_+ + (I_-)_3(\Delta\epsilon_-)_3 t_-}{t_+ + t_-}$$

$$+ \frac{(I_+)_3(\epsilon_+')_3 t_+ + (I_-)_3(\epsilon_-')t_-}{t_+ + t_-}\left(\frac{d_2 - L_1}{d_2 + d_3}\right)$$

$$= (25)\frac{(3.9)(19)+(9.6)(4)}{(19)+(4)} + \frac{(195)(3.9)(19)+(200)(9.6)(4)}{(19)+(4)}$$

$$+ \frac{(195)(14.1)(19)+(200)(27.4)(4)}{(19)+(4)}\left(\frac{0.178-0.133}{0.178+0.22}\right)$$

$$= 122.28 + 962.15 + (3224.4)(0.113) = 1448.79 \text{ W} \qquad (4\text{-}1)$$

Plasma arc power loss through the nozzle ($\dot{q}_A$) can be computed from the summation of heat convection, $h_A A(T_{plasma} - T_W)$; free electron loss, $(I_1/e)[(3/2)kT^*]$; and power loss due to difference in anode potential and plasma column drop of argon gas at nozzle, $I_1\phi_1$, namely

$$\dot{q}_A = h_A A(T_{plasma} - T_W) + \frac{I_1}{e}\left(\frac{3}{2}kT^*\right) + I_1\phi_1 \qquad (4\text{-}2)$$

where h_A stands the film coefficient; A, the circumferential area of the nozzle; T_{plasma}, the plasma gas temperature; T_W, the wall temperature of the nozzle; e, electric charge of electron; k (=1.38 x 10^{-16}erg/mole·^{0}K), the Boltzmann constant; T*, the average temperature between plasma gas and the surface of nozzle; and ϕ_1, the average difference in anode potential and plasma column drop of argon gas.

(A) Calculation of Film Coefficient h_A

Heat transfer equation for plasma flow in a tube from Hsu and Rubinsky (1987) gives

$$N_u = 0.2233\ (X^+)^{-0.7455} + 3.66 \qquad (4\text{-}3)$$

where

$$X^+ = \frac{x}{R}\ \frac{1}{(R_e P_r)_m} \qquad (4\text{-}4)$$

$$N_u = \frac{hD}{k} = \text{Nussel Number} \qquad (4\text{-}5)$$

$$R_e = \frac{uD}{\mu} = \text{Reynolds Number} \qquad (4\text{-}6)$$

$$P_r = \frac{C_p \mu}{k} = \text{Prandtl Number} \qquad (4\text{-}7)$$

Here, x denotes the distance in axial coordinate; R, the radius of tube; h, the convective heat transfer coefficient (or film coefficient); D (=2R), the diameter of the tube; k, the heat conduction coefficient; u, the flow velocity of plasma gas; μ, the viscous coefficient; and C_p, the constant pressure specific heat. Substituting Equations (4-4) and (4-5) in Equation (4-3), we have

$$h = \frac{k}{R}\left\{(0.1116)\left(\frac{R\ R_e\ P_r}{x}\right)^{0.7455} + 1.83\right\} \qquad (4\text{-}8)$$

Define $\bar{h}$ as the average heat transfer coefficient along the axial distance of nozzle. After substituting Equations (4-6) and (4-7) in Equation (4-8), it leads

$$\bar{h} = \frac{1}{L}\int_0^L h\,dx$$

$$= \frac{k}{R}\left\{(0.4385)\left(\frac{2\dot{m}C_p}{\pi L k}\right)^{0.7455} + 1.83\right\} \qquad (4\text{-}9)$$

(B) Determination of Plasma Temperature at the Nozzle Entrance of Argon Plasma Gas

Argon Plasma gas enthalpy $(h)_p^a$ at the nozzle entrance can be obtained as

$$(h)_p^a = \frac{P_a}{\dot{m}} = \left(\frac{1448.79\ J/s}{9.585 \times 10^{-2}\ g/s}\right)(0.239\ cal/J)$$

$$= 3612.5\ cal/g \qquad (4\text{-}10)$$

As the enthalpy is a function of temperature, the argon plasma gas temperature T_a at the nozzle entrance can be determined from the Table

shown in Drellishak et al. (1963), namely

T_a = 12600 °K

(C) Plasma Arc Power Loss Due to Convective Heat Transfer

In order to determine the convective heat transfer loss, one has to understand the temperature profile of flow field. In other words, the iteration process has to carry out by assuming the temperature profile of the flow field for the calculation of convective heat trasfer loss. Temperature profile of the flow field can be checked from the calculated heat transfer loss, and vice versa. In this case, argon plasma jet temperature at the outlet end of nozzle is

T_b = 8760 °K

Average temperature of argon plasma flow through the nozzle is

$\bar{T}$ = 1/2(12600 + 8760) = 10680 °K

Coefficients of argon plasma gas properties (at the temperature of 10680 °K) and nozzle (surface temperature is assumed to be T_W = 1000 °K) can be determined from Drellishak et al (1963) and Lancaster (1986), as follows:

k = 0.85348 J/m·s·°K

C_p = 0.5418 cal/g·°K

μ = 2.8592 x 10^{-4} kg/m·s

Thus, we can calculate Reynolds number, Prandtl number, average film coefficient, and convective heat transfer loss as follows:

$$R_e = \frac{uD}{\mu} = \frac{\rho uD}{\mu} = \frac{\dot{m}D}{\mu A} = \frac{\dot{m}D}{\mu(\pi/4)D^2} = \frac{4\dot{m}}{\pi D\mu}$$

$$= \frac{(4)(9.585 \times 10^{-2}\ g/s)(10^{-3}\ kg/g)}{(\pi)(0.1562in)(2.54cm/in)(2.8592 \times 10^{-4} kg/m\cdot s)(10^{-2} m/cm)}$$

$$= 107.6$$

$$P_r = \frac{C_p \mu}{k}$$

$$= \frac{(0.5418 cal/g\cdot{}^\circ K)(4.1868 J/cal)(10^3 g/kg)(2.8592 \times 10^{-4} kg/m\cdot s)}{(0.85348\ J/m\cdot s\cdot{}^\circ K)}$$

$$= 0.76$$

$$\bar{h}_A = \frac{k}{R}\left\{(0.4385)\left(\frac{2\dot{m}C_p}{\pi Lk}\right)^{0.7455} + (1.83)\right\}$$

$$= \left(\frac{0.85348\ J/m\cdot s\cdot{}^\circ K}{\left(\frac{0.1562}{2}\right)(2.54)cm}\right)(10^{-2} m/cm)\left\{(0.4385)\right.$$

$$\left.\cdot\left[\frac{(2)(9.585 \times 10^{-2}\ g/s)(0.5418\ cal/g\cdot{}^\circ K)}{(\pi)(0.133 \times 2.54\ cm)(0.85348\ J/m\cdot s\cdot{}^\circ K)}\right.\right.$$

$$\left.\left.\cdot\left.\frac{(4.1868\ J/cal)}{(10^{-2}\ m/cm)}\right]^{0.7455} + (1.83)\right\}$$

$$= 0.41676\ J/cm^2\cdot s\cdot{}^\circ K$$

Convective Heat Loss $= \bar{h}_A A(\bar{T}-T_W)$

$$= (0.41676)[\pi(0.1562)(0.133)(2.54)^2](10680 - 1000)$$

$$= 1761.75\ W$$

(D) Plasma Arc Power Loss Due to Free Electrons

The vapor temperature on the surface of nozzle can be considered to be 3000°K (Metcalfe and Quigley, 1975). Thus, the average temperature between argon plasma gas temperature and vapor

temperature on the surface of nozzle is

$$T^* = 1/2(3000 + 10680) = 6840^\circ K$$

$$\text{Free Electron Loss} = \frac{I_1}{e}\left(\frac{3}{2} kT^*\right)$$

$$= \frac{(25 \text{ coulomb/s})}{(1.602 \times 10^{-19} \text{ coulomb/molecule})}\left(\frac{3}{2}\right)$$

$$\cdot (1.38 \times 10^{-16} \text{ erg/mol}\cdot^\circ K)(6840^\circ K)$$

$$= 2.21 \times 10^8 \text{ erg/s} = 22.1 \text{ W}$$

(E) Plasma Arc Power Loss Due to Difference in Anode Potential and Argon Plasma Gas Column Drop at Nozzle

Average plasma arc power loss due to the difference in anode potential and argon plasma gas column drop at nozzle can be shown as

$$I_1\phi_1 = I_1\frac{(\Delta\epsilon_+')t_+ + (\Delta\epsilon_-')t_-}{t_+ + t_-}$$

where

$$(\Delta\epsilon_+') = (\epsilon_{+a})_n - (\epsilon_+)_n$$

$$(\Delta\epsilon_-') = (\epsilon_{-a})_n - (\epsilon_-)_n$$

$$(\epsilon_+)_n = (\epsilon_+)_{c,g} + (\epsilon_d)(d_2 - L_1)$$

$$(\epsilon_{+a})_n = (\epsilon_+)_{c,e} + (\epsilon_+)_1$$

$$(\epsilon_-)_n = (\epsilon_-)_{c,g} - (\epsilon_d)(d_2 - L_1)$$

$$(\epsilon_{-a})_n = (\epsilon_-)_{c,e} + (\epsilon_-)_1$$

Here, $(\epsilon_+)_{c,g}$ denotes argon plasma gas electric potential in the neighborhood of electrode (cathode) during the straight polarity; ϵ_d, column drop of argon plasma gas; $(\epsilon_+)_{c,e}$, electric potential of electrode (cathode) during the straight polarity; $(\epsilon_-)_{c,g}$, argon plasma gas electric potential in the neighborhood of electrode

(anode) during the reverse polarity; and $(\epsilon_-)_{c,e}$, electric potential of electrode (anode) during the reverse polarity. For the VPPA welding system operated in the NASA/MSFC, following values are given:

$(\epsilon_+)_{c,g} = -25.3$ V, $\epsilon_d = 35.5$ V/in

$d_2 - L_1 = 0.045$ in, $(\epsilon_+)_{c,e} = -29.2$ V

$(\epsilon_+)_1 = 17$ V $(\epsilon_-)_{c,g} = 29.7$ V

$(\epsilon_-)_{c,e} = 39.3$ V, $(\epsilon_-)_1 = 0.3$ V

Thus,

$$(\epsilon_+)_n = (\epsilon_+)_{c,g} + \epsilon_d(d_2 - L_1)$$
$$= -25.3 + (35.5)(0.045) = -23.7 \text{ V}$$

$$(\epsilon_{+a})_n = (\epsilon_+)_{c,e} + (\epsilon_+)_1$$
$$= -29.2 + 17 = -12.2 \text{ V}$$

$$(\epsilon_-)_n = (\epsilon_-)_{c,g} - \epsilon_d(d_2 - L_1)$$
$$= 29.7 - (35.5)(0.045) = 28.1 \text{ V}$$

$$(\epsilon_{-a})_n = (\epsilon_-)_{c,e} + (\epsilon_-)_1$$
$$= 39.3 + 0.3 = 39.6 \text{ V}$$

$$(\Delta\epsilon_+') = (\epsilon_{+a})_n - (\epsilon_-)_n$$
$$= -12.2 + 23.7 = 11.5 \text{ V}$$

$$(\Delta\epsilon_-') = (\epsilon_{-a})_n - (\epsilon_-)_n$$
$$= 39.6 - 28.1 = 1.5\text{V}$$

Therefore,

$$I_1\phi_1 = I_1\frac{(\Delta\epsilon_+')t_+ + (\Delta\epsilon_-')t_-}{t_+ + t_-}$$

$$= (25)\frac{(11.5)(19) + (1.5)(4)}{(19) + (4)} = 287.5 \text{ W}$$

(F) Plasma Arc Power Loss Through Nozzle

$$\dot{q}_A = \bar{h}_A A(\bar{T}-T_W) + \frac{I_1}{e}\left(\frac{3}{2}kT^*\right) + I_1\phi_1$$

$$= 1761.75 + 22.1 + 287.5 = 2071.35 \text{ W}$$

(G) Percentage of Plasma Arc Power Loss Through Nozzle

Among the plasma arc power loss in the whole VPPA welding system, the percentage of power loss through the nozzle is:

$$\frac{\dot{q}_A}{P} = \frac{2071.35}{6979.13} = 29.6\%$$

for the VPPA welding system operated at the NASA/MSFC.

V. Plasma Arc Power Loss Between the Outlet of Nozzle to the Inlet of Keyhole in Workpiece

Flow pattern of argon plasma gas between the outlet of nozzle to the inlet of keyhole in workpiece is a plasma gas column jet stream.

(A) Plasma Arc Power at the Outlet End of Nozzle

Estimation of plasma arc power distribution is again based on the linear power distribution assumption. This can be calculated as follows:

$$P_b = P_a + I_3(\epsilon')_3\left(\frac{L_1}{d_2 + d_3}\right) - \dot{q}_A$$

$$= 1448.79 + (3224.4)\left(\frac{0.133}{0.178 + 0.22}\right) - 2071.35$$

$$= 454.94 \text{ W}$$

Argon plasma gas enthalpy $(h)_p^b$ at the outlet of nozzle can be obtained as

$$(h)_p^b = \frac{P_b}{\dot{m}} = \frac{(454.94 \text{ J/s})}{(9.585 \times 10^{-2} \text{ g/s})}(0.239 \text{ cal/J}) = 1134.4 \text{ cal/g}$$

Argon plasma gas temperature at the outlet of nozzle, T_b, can be determined from table shown in Drellishak et al. (1963), i.e.,

$T_b = 8750°K$

(B) Plasma Arc Power Loss Between the Outlet End of Nozzle to The Inlet End of Workpiece

Following assumptions are made for proceeding the mathematical formulation:

(1) Major power loss in this region consists of radiative heat transfer loss and convective heat transfer loss.

(2) Equally divided plasma flow path into 5 segments between the outlet end of nozzle to the inlet end of workpiece

Calculations procedures for Segment 1 is illustrated. Results of the whole flow fields for the five segments are shown in Table 1. Computation methods for the rest of four segments are similar to that of Segment 1 shown in this report.

(B-1) Plasma Arc Column Radiative Heat Transfer Loss for Segment 1

Radiative Heat Flux for Segment 1 can be shown in the following equation

$$\dot{Q}_{R1} = \sigma \epsilon A_1 (T^4_{plasma,1} - 300^4)$$

where $\sigma = 5.67 \times 10^{-8}$ W/m^{2}K^4, is Stefan-Boltzmann constant. Note that argon plasma arc temperature is greater than 10^4 K which is several orders of magnitude greater than the surrounding medium temperature. Therefore, the emmissivity of radiation from the surrounding is negligible in the present case. The value of emmissivity can be

chosen from Metcalfe and Quigley (1975) which is $\epsilon = 0.02247$. In the meanwhile, the surrounding area of the argon plasma arc column is

$$A_1 = (\pi d_1)\left(\frac{d_3}{5}\right) = [\pi(0.1562)(2.54)]\left[\frac{1}{5}(0.22)(2.54)\right]$$

$$= 0.1393 \text{ cm}^2$$

The inlet temperature of the plasma arc column is equal to the outlet end of nozzle,

$$T_{1,e} = T_b = 8750°K$$

The outlet end temperature of Segment 1 plasma arc column $T_{1,0}$, has to assume. Let us assume $T_{1,0} = 10350°K$. The average temperature of Segment 1 is, thus

$$\bar{T}_1 = \frac{1}{2}(8750 + 10350) = 9550°K$$

The value of C_p can be obtained from this temperature,

$$C_p(9550°K) = 0.278 \text{ cal/g}\cdot°K$$

Plasma arc column radiative heat loss for Segment 1 is, thus,

$$\dot{Q}_{R1} = \sigma\epsilon A_1(\bar{T}_1^4 - 300^4)$$

$$= (5.67 \times 10^{-8} \text{ W/m}^2\cdot\text{K}^4)(10^{-4} \text{ m}^2/\text{cm}^2)(0.02247)$$

$$\cdot (0.1393 \text{ cm}^2)(9550^4 - 300^4)$$

$$= 147.61 \text{ W}$$

(B-2) Comparison of Plasma Jet Velocity and Shielding Gas Velocity

(a) Plasma Jet Velocity

At the outlet end of nozzle, argon plasma temperature is T = 8750°K, and density of plasma is $\rho = 5.5355 \times 10^{-5}$ g/cm^3. We can determine the cross sectional area of plasma arc column,

$$A = \frac{\pi}{4} D^2 = \frac{\pi}{4} [(0.1562)(2.54)]^2 = 0.12363 \text{ cm}^2$$

Argon plasma jet velocity can be calculated from the conservation of mass flow rate, $\dot{m} = \rho u_p A$. Thus, we have the plasma jet velocity

$$u_p = \frac{\dot{m}}{\rho A} = \frac{(9.585 \times 10^{-2} \text{ g/s})(10^{-2} \text{ m/cm})}{(5.5355 \times 10^{-5} \text{ g/cm}^3)(o.12363 \text{ cm}^2)} = 140.1 \text{ m/s}$$

(b) Shielding Gas Velocity

Volumetric flow rate for helium shielding gas of VPPA welding system operated by the NASA/MSFC is $\dot{Q}_{sg} = 35 \text{ ft}^3/\text{hr}$ at 25°C. We can convert the present units to cm^3/s from following relation

$$\dot{Q}_{sg} = (35 \text{ ft}^3/\text{h})\left(\frac{1}{3600} \text{hr/s}\right)(35.3147 \text{ m}^3/\text{ft}^3)(10^6 \text{ cm}^3/\text{m}^3)$$

$$= 275.3 \text{ cm}^3/\text{s}$$

Based on the equation of state, we have

$$P = \rho \frac{R}{M} T$$

where M (=4.003 g/mol for helium) denotes molecular weight. One can calculate the density of helium from the following relation

$$(1 \text{ atm}) = \rho \frac{(82.05 \text{ cm}^3 \cdot \text{atm/mole} \cdot {}^\circ\text{K})}{(4.003 \text{ g/mol})} (298 {}^\circ\text{K})$$

Therefore, we have helium density

$$\rho_{He} = 1.637 \times 10^{-4} \text{ g/cm}^3$$

Mass flow rate of helium is

$$\dot{m}_{sg} = \rho_{He} \dot{Q}_{sg} = (275.3 \text{ cm}^3/\text{s})(1.637 \times 10^{-4} \text{ g/cm}^3)$$

$$= 4.5071 \times 10^{-2} \text{ g/s}$$

Cross-sectional flow area of shielding gas is

$$A_{sg}^* = \frac{\pi}{4}(D_1^2 - D^2) = \frac{\pi}{4}[\{(0.709)(2.54)\}^2 - \{(0.1562)(2.54)\}^2]$$

$$= 2.4235 \text{ cm}^2$$

Again, shielding gas velocity u_s can be computed from the conservation of mass flow rate, $\dot{m}_{sg} = \rho_{He} u_s A_{sg}^*$. It leads

$$u_s = \frac{\dot{m}_{sg}}{\rho A_{sg}^*} = \frac{(4.5071 \times 10^{-2} \text{ g/s})(10^{-2} \text{ m/cm})}{(1.637 \times 10^{-4} \text{ g/cm}^3)(2.4235 \text{ cm}^2)} = 1.136 \text{ m/s}$$

The ratio of shielding gas velocity to plasma jet velocity is

$$\frac{u_s}{u_p} = \frac{1.136}{140.1} = 8.1 \times 10^{-3}$$

Therefore, the effect of shielding gas velocity in the flow zone calculation of plasma arc jet can be ignored.

(B-3) Plasma Arc Jet Convective Heat Transfer Loss for Segment 1

Surrounding the high temperature argon plasma jet, there is low temperature helium shielding gas. We are not going to encounter with the dissociation problem for the shielding gas since helium is monoatomic. Based on Ibele (1963) the neutral helium gas begins to break up toward ionization at 1 atm in the neighborhood of 13000 to 15000 °K, and produces helium ions and electrons. In this particular case, the consideration of the ionization of helium gas is not necessary because the plasma jet temperature is below the temperature required for the ionization of helium gas.

Based on Abramovich (1963) for the arc column convective heat

transfer loss for turbulent jet, it shows that the convective heat flux is

$$\dot{Q}_{c1} = 48A_1 \rho u_p C_p \Delta T$$

Numerical constant in the equation is resulted from the length scale factor of the edge of turbulent jet column. A_1 is the surrounding area of plasma column; u_p, the plasma jet velocity; and ΔT, the temperature difference between plasma jet and surrounding gas. Thus, we can calculate plasma arc column convective heat transfer loss for segment 1 as follows:

$$\dot{Q}_{c1} = 48A_1 \rho u C_p \Delta T = \frac{48}{3600} \frac{A_1}{A_c} \dot{m} C_p \Delta T$$

$$= \frac{48}{3600} \frac{(0.1393\ cm^2)}{(0.1236\ cm^2)} (9.585 \times 10^{-2}\ g/s)(0.278\ cal/g \cdot {}^{\circ}K)$$

$$\cdot (4.1868\ J/cal)(9550 - 300) = 15.51\ Watts$$

Here, A_1 stands cross sectional area of the plasma arc column.

(B-4) Total Plasma Arc Column Power Loss of Segment 1

Total plasma arc column power loss of segment 1 is a summation of radiative heat transfer and convective heat transfer losses, namely

$$\dot{Q}_1 = \dot{Q}_{R1} + \dot{Q}_{C1} = 147.61 + 15.51 = 163.12\ W$$

(B-5) Plasma Arc Power at Outlet End of Segment 1

$$P_1 = P_b + I_3 \epsilon' \frac{(d_2/5)}{d_2 + d_3} - \dot{Q}_1$$

$$= 454.94 + (3224.4)\left(\frac{0.044}{0.178 + 0.22}\right) - 163.12$$

$= 648.28$ W

Enthalpy of argon plasma jet at the outlet end of Segment 1 is

$$h_1 = \frac{P_1}{\dot{m}} = \frac{(648.28 \text{ J/s})}{(9.585 \times 10^{-2} \text{ g/s})}(0.239 \text{ cal/J})$$

$= 1616.5$ cal/g

Thus, argon plasma jet temperature at the outlet end of Segment 1 can be obtained from the table shown in Drellishak et al. (1963), i.e.,

$T_{i,0} = 10370°K$

Similarly, the computational methods for physical parameters obtained for Segment 1 can be carried out for Segments 2 to 5. Table 1 shows the listings of computed physical parameters for Segments 1 to 5.

(B-6) Percentage of Plasma Arc Power Loss Between Outlet End of Nozzle to Inlet End of Keyhole

Plasma arc power losses, P_i^L from Segments 1 to 5 are illustrated in Table 1. Percentage of plasma arc power loss between outlet end of nozzle to inlet end of keyhole can be determined from the summation of power losses from Segments 1 to 5 divided by the total power of the VPPA system which is

$$\frac{q_b}{P} = \frac{P_1^L + P_2^L + P_3^L + P_4^L + P_5^L}{P} = \frac{1371}{6979.13} = 20\%$$

VI. Plasma Arc Power Loss Through Keyhole

Plasma arc jet power at the entrance point of keyhole is

$$P_C = P_5 + \frac{(I_+)_3(\Delta\epsilon_+')_3 t_+ + (I_-)_3(\Delta\epsilon_-')_3 t_-}{t_+ + t_-} \qquad (6\text{-}1)$$

$$= 866.5\ W + \frac{1}{(19 + 4\ s)}\Big[(195\ \text{coulomb/s})(11.2\ V)(19\ s) +$$

$$+ (200\ \text{coulomb/s})(2.3\ V)(4\ s)\Big]$$

$$= 8.66.5\ W + 1884.17\ W = 2750.67\ W$$

Here, $(\Delta\epsilon_+')_3$ denotes the workfunction and anode drop of workpiece, shown in Figure 4; and $(\Delta\epsilon_-')_3$ shows the workfunction and cathode drop of workpiece, also shown in Figure 4. For the system operated at NASA/MSFC, $(\Delta\epsilon_+')_3$ is 11.2V and $(\Delta\epsilon_-')_3$ is 2.3V.

Enthalpy of argon plasma jet at the entrance point of keyhole can be determined by

$$h_C = \frac{P_C}{\dot{m}} = \frac{(2750.67\ J/s)}{(9.585 \times 10^{-2}\ g/s)}(0.239\ cal/J) = 6858.74\ cal/g$$

Thus, argon plasma jet temperature and density at the entrance point of keyhole can be obtained from the tables shown in Drellishak et al. (1963), i.e.,

$$T_c = 14280°K\ ;\ \rho_c(T=14280°K) = 2.3564 \times 10^{-5}\ g/cm^3$$

(A) Penetration Depth of Keyhole Due to Argon Plasma Jet

Based on Lancaster (1986), pressure acting on the free surface of the liquid at the bottom of keyhole can be considered such that the stagnation pressure due to the plasma jet shall be balanced by the surface tension and hydrostatic head, namely

$$P_s = \rho_m g h + \frac{2\sigma}{R} \qquad (6\text{-}2)$$

where P_s is the stagnation pressure due to plasma arc jet; ρ_m, metal

density of workpiece; σ, the surface tension of liquid metal of workpice; and R, the radius of curvature at the root of penetration. In the case of VPPA welding system operated at NASA/MSFC, by using AL #2219 as a workpiece, values of material properties can be obtained as follows (American Society for Metal Handbook Committee, 1979; Robert and Melvin, 1981): $\rho_m = 2.84\ g/cm^3$, and σ(at melting temperature of AL #2219 for wall temperature $T_w = 916.67°K$) = 0.865 N/m. The stagnation pressure due to the plasma arc jet can be shown as

$$P_s = \frac{1}{2}\rho_g u^2 = \frac{1}{2}\frac{(\rho uA)^2}{\rho A^2} = \frac{1}{2}\frac{\dot{m}^2}{\rho A^2}$$

Thus, the minimum penetration depth h becomes

$$h = \frac{P_s - \frac{2\sigma}{R}}{\rho_m g} = \frac{\frac{1}{2}\frac{\dot{m}^2}{\rho A^2} - \frac{2\sigma}{R}}{\rho_m g} \qquad (6\text{-}3)$$

$$= \left[\frac{1}{2}\frac{(9.585 \times 10^{-2}\ g/s)^2}{(2.3564 \times 10^{-5}\ g/cm^3)(0.12363\ cm^2)^2} - \frac{(2)(0.865\ N/m)(10^3\ g\cdot m\cdot s^{-2}/N)}{(1/2)[(0.1562)(2.54)cm]}\right] / \left[(2.84\ g/cm^3)(9.8\ m/s^2)(10^2\ cm/m)\right]^{-1}$$

$$= 1.4492\ cm = 0.57\ inch \qquad (6\text{-}4)$$

In our case, the thickness of workpiece is 0.375 in. which is smaller than 0.57 in. In other words, the thrust force induced by the plasma arc jet can penetrate the workpiece completely.

Note that the result of penetration depth shown in this analysis is strictly based upon the dynamics of the computation of fluid mechanics which can provide the necessary condition, but <u>not</u> the

sufficient condition. As the plasma arc temperature is several orders of magnitude greater than the melting temperature of metal, it can assure that the penetration depth of 0.57 in, which is greater than the thickness of workpiece (0.375 in.), can be carried out and the plasma arc jet can penetrate the workpiece completely.

Further discussion of the sufficient condition as to whether the power of plasma is large enough to provide the thermal energy for melting the workpiece will be accomplished in Section (VI-E).

(B) Convective Heat Transfer Loss for Partial Penetration of Workpiece

There are two kinds of convective heat transfer on the workpiece. At the beginning before a keyhole is formed, plasma arc jet impinges perpendicularly on the surface of the weld pool, and is deflected across the weld surface radially away from the stagnation point (see Figure 5). Once a keyhole is formed, a significant amount of plasma gas will pass through the keyhole, and discharge to the other side of the workpiece.

(B-1) Weld Pool Convective Heat Transfer

Governing equation of weld pool convective heat transfer, in particular for flow with impingement, can be shown from Metcalfe and Quigley (1975),

$$Nu = 0.78\ Re^{0.5}\ Pr^{0.33} \qquad (6\text{-}5)$$

Again, Nu stands for the Nussett number; Re, the Reynolds number; and Pr, the Prandtl number. Radius of the area of impingement is assumed to be twice the radius of the plasma arc jet. Average temperature is taken between the ethalpys of plasma arc and that of weld pool which

are the function of temperature. The enthalpy average is given by

$$\bar{H}(\bar{T}) = 1/2[H_{arc}(T_a) + H_{weld\ pool}(T_{wp})] \qquad (6\text{-}6)$$

Now, from the available VPPA welding system operated at NASA/MSFC, we have

$$H_{arc}(T_a) = h_c = 6858.74\ cal/g = 28.716\ MJ/kg$$

$$H_{wp}(T_{wp}) = 0.3672\ MJ/kg$$

where $T_{wp} = 916°K$ is the melting temperature of workpiece.

Thus, the enthalpy average is

$$\bar{H}(\bar{T}) = 1/2(28.716 + 0.3672) = 14.5417\ MJ/kg$$

From tables shown in Drellishak et al. (1963), we have the average plasma arc jet temperature $T = 12456°K$. Also, we have the values of physical parameters at this temperature range as follows: $C_p = 5.8461\ J/g\cdot°K$, $\rho = 33.576\ g/m^3$, $\mu = 188.6 \times 10^{-3}\ g/m^3$ and $k = 3.1104\ W/m\cdot K$. We can calculate the velocity of plasma arc jet, Reynolds number and Prandtl number as follows:

$$u = \frac{\dot{m}}{\rho_g A} = \frac{(9.585 \times 10^{-2}\ g/s)(10^{-2}\ m/cm)}{(2.3564 \times 10^{-5}\ g/cm^3)(0.12363\ cm^2)} = 329\ m/s$$

$$R_e = \frac{\rho u D}{\mu} = \frac{(33.567\ g/m^3)(329\ m/s)(0.1562 \times 2.54\ cm)(10^{-2}\ m/cm)}{(188.6 \times 10^{-3}\ g/m\cdot s)}$$

$$= 232.33$$

$$P_r = \frac{C_p \mu}{k} = \frac{(5.8461\ J/g\cdot k)(188.6 \times 10^{-3}\ g/m\cdot s)}{(3.1104\ W/m\cdot K)} = 0.35448$$

Substituting the values of Reynolds number and Prandtl number in the heat transfer equation, we can determine the Nusselt number for the heat transfer flow field,

$$N_u = 0.78 R_e^{0.5} P_r^{0.33} = (0.78)(232.33)^{0.5}(0.35448)^{0.33}$$

$$= 8.4142$$

From the definition of Nusselt number, the coefficient of heat convection can be determined

$$h = \frac{N_u k}{D} = \frac{(8.4142)(3.1104\ W/m\cdot k)(10^{-2}\ m/cm)}{[(0.1562)(2.54)cm]} = 0.65964\ W/cm^2$$

Thus, the plasma gas power loss for the partial penetration of arc jet through the weld pool is

$$Q = hA\frac{\Delta H}{C_p} \qquad (6\text{-}7)$$

$$= (0.65964\ W/cm^2\cdot K)[\pi/4((0.1562)(2.54)cm)^2]$$

$$\cdot\ [28.716-0.3672)\ x\ 10^3\ J/g]\ \cdot\ (5.8461\ J/g\cdot K)^{-1}$$

$$= 1582\ W$$

Percentage of plasma arc power loss for <u>partial</u> <u>penetration</u> through the weld pool is

$$\frac{Q}{P} = \frac{1582}{6979.13} = 23\%$$

(B-2) Convective Heat Transfer Through the Wall of Keyhole

Recent study indicates that heat transfer rate out of the rear half of a keyhole is less than that of the front half. This implies that more heat transfer area is required for the front half than that of the rear half. In fact, the shape of keyhole with which plasma gas actually contact and transfer heat energy is like a finger ring. This ring-shaped geometry can be simplified and expanded into the drawing shown in Figure 6.

Surface of keyhole has been equally divided into 5 segments along the axis of keyhole between the inlet end and outlet end. Calculation

procedures of heat convection for Segment 1 is illustrated. Results of the rest of the four segments are shown in the Table 2. Computation methods are all similar to that of Segment 1.

(1) Geometry for Segment 1

Figure 6 shows the illustration of geometrical parameters. From the available data of VPPA welding system, operated at NASA/MSFC, we can compute the geometrical parameters as follows:

$$a_1 = \pi r = (\pi)\left\{\frac{(0.1562)(2.54)}{2}\right\} = 0.6232 \text{ cm}$$

$$\alpha^\circ = \tan^{-1}\left(\frac{\frac{1}{2} - L_2}{\frac{\pi}{2} - r}\right) = \tan^{-1}\left(\frac{0.375}{\left(\frac{\pi}{2}\right) - (0.1562)}\right) = 56.8^\circ$$

$$a_2 = a_1 + 2\frac{L}{\tan\alpha^\circ} = 0.6232 + 2\left(\frac{(0.375)(2.54)}{5}\right)\frac{1}{\tan(56.8^\circ)}$$

$$= 0.8725 \text{ cm}$$

$$\text{Area} = \frac{1}{2}(a_1 + a_2)L = \left(\frac{1}{2}\right)(0.6232 + 0.875)\left(\frac{(0.375)(2.54)}{5}\right)$$

$$= 0.14247 \text{ cm}^2$$

(2) Convective Heat Transfer for Segment 1

The governing equation of convective heat transfer for Segment 1 can be obtained from Metcalfe and Quigley (1975). It leads

$$\bar{N}_u = 0.664\ R_e^{0.5} P_r^{0.33} \qquad (6\text{-}8)$$

where $\bar{N}_u$ stands for average Nusselt number; R_e, the Reynolds number; and P_r, the Prandtl number.

It is noted that heat transfer equation for plasma flow in a tube from Hsu and Rubinsky (1987) was used to compute the convective heat

transfer of plasma gas flowing through circular tube-like nozzle, shown in Equations (4-3) and (4-8). There are great differences for flow patterns between plasma gas through nozzle and that of plasma gas through workpiece. These differences are as follows: (1) Nozzle is always a solid circular wall while keyhole of workpiece is constantly a wall with molten metal rather than a pure solid wall; and (2) Cross-section of keyhole is a curved surface like a finger ring-shaped rather than a cylindrical or conical-shaped as that of nozzle. This makes that Equation (6-8) is different from Equation (4-3). Furthermore, the difference in convective heat transfer equations between Equations (6-5) and (6-8) are due to the fact that Equation (6-6) is applicable to impingement type flow pattern convective heat transfer plasma gas in a molten metal wall of workpiece while that of Equation (6-8) is suitable for plasma gas flowing in a molten metal wall with completed penetration.

Plasma gas enthalpy at the inlet end of Segment 1 is equal to the plasma gas enthalpy at the entrance of keyhole

$$H_{1,i} = h_c = 28.716 \text{ MJ/kg}$$

Again, the iteration process is needed to carry out by assuming the temperature profile of the flow field. Assuming plasma gas enthalpy at the outlet end of Segment 1 is

$$H_{1,0} = 24.1255 \text{ MJ/kg}$$

Thus, the average enthalpy of plasma arc jet between inlet and outlet ends of Segment 1 is

$$H_{1,m} = 1/2(H_{1,0} + H_{1,i}) = 1/2(24.1255 + 28.716)$$
$$= 26.421 \text{ MJ/kg}$$

Furthermore, the average enthalpy of boundary layer between the average enthalpy of the main flow of plasma arc jet and the wall enthalpy of workpiece is

$$\bar{H}_1 = 1/2(H_{1,m} + H_{1,w}) = 1/2(26.421 + 0.3672)$$
$$= 13.394 \text{ MJ/kg}$$

The corresponding average temperature for the enthalpy can be determined from the table shown in Drellishak et al (1963) which is

$$\bar{T}_1 = 12263^\circ K$$

Physical parameters of flow fields at this temperature are as follows: $C_p = 5.351$ J/g·°K, $\rho = 34.694$ g/m^3, $\mu = 193.425 \times 10^{-3}$ g/m·s, $k = 2.937$ W/m·°K.

We can calculate the corresponding Reynolds number and Prandtl number as follows:

$$R_e = \frac{\dot{m}L}{\mu A} = \frac{(0.0985 \text{ g/s})[(0.1905 \text{ cm})(10^2 \text{ cm/m})}{(193.425 \times 10^{-3} \text{ g/m·s})(0.12363 \text{ cm}^2)} = 76.36$$

$$P_r = \frac{\mu C_p}{k} = \frac{(193.425 \times 10^{-3} \text{ g/m·s})(5.351 \text{ J/g·°K})}{(2.937 \text{ W/m·°K})} = 0.3524$$

Substituting the obtained values of R_e and P_r in the governing equation, we have the mean Nusselt number for the flow field

$$\bar{N}_u = 0.664 R_e^{0.5} P_r^{0.33}$$
$$= (0.664)(76.36)^{0.5}(0.3524)^{0.33} = 4.099$$

From the definition of Nusselt number, we can determine the mean value of heat covection coefficient

$$\bar{h} = \frac{k\bar{N}_u}{L} = \frac{(2.937 \text{ W/m·°K})(4.099)}{(0.1905 \text{ cm})}(10^{-2} \text{ m/cm})$$
$$= 0.632 \text{ J/cm}^2\text{·s·°K}$$

Plasma arc power loss at Segment 1 can be determined by

$$P_1 = \frac{hA\Delta H}{C_p}$$

$$= \frac{(0.632 J/cm^2 \cdot s \cdot K)(0.14247 cm^2)[(26.421 - 0.3672)x10^3 J/g]}{(5.351\ J/g \cdot {}^0K)}$$

$$= 439\ W$$

This result is agreeable with the value computed from $\dot{m}(H_{1,i} - H_{1,o})$. Table 2 shows the computed convective heat transfer loss from Segments 1 to 5 which are checked with the corresponding enthalpy difference between the inlet end and outlet end of each corresponding segment.

(3) Percentage of Plasma Arc Power Loss Through the Workpiece

Total plasma arc power loss through the workpiece is the summation of power loss for Segments 1 to 5, shown in Table 2. Thus, the percentage of plasma arc power loss through the workpiece can be determined. It is

$$\frac{P_1 + P_2 + P_3 + P_4 + P_5}{P}$$

$$= \frac{439 + 497 + 494 + 350 + 211}{6979} = \frac{1991}{6979} = 28.5\%$$

(C) Temperature at the Outlet End of Workpiece

From Table 2, we have the enthalpy for the outlet end of Segment 5 of the workpiece

$$H_{5,o} = 7.923\ MJ/kg$$

The corresponding plasma arc temperature at the outlet end of workpiece, thus, can be determined from the computed enthalpy based on the table shown in Drellishak et al. (1963)

$T_{5,0} = 10870°K = T_d$

(D) Calculation of the Puddle Width

Surface of the keyhole has been equally divided into 5 segments along the axis of keyhole between the inlet end and outlet end. As the temperature gradient along the axial keyhole direction of the workpiece is usually negligible at every segment, heat flow during the time period of welding can be assumed to be two-dimensional. The steady state, two dimensional heat flow during the course of welding of thin sheet was first analyzed by Rosenthal (1941). However, the temperature gradient along the axial keyhole direction becomes important when we are interested in computing crown width and height together with root width and height. In other words, three-dimensional heat flow shall be considered when one is particularly interested in the relation between crown and root sections of welding. In this study, a moving coordinate system is adopted and shown in Figure 7.

Following assumptions are made for the mathematical formulations: (1) No melting and no heat fusion is involved; (2) thermal properties of the workpiece are constant; (3) there is no heat loss from the surface of workpiece due to the radiation or convective heat transfers; and (4) a point heat source is assumed.

The governing equation for three-dimensional heat conduction is given by

$$\alpha\left(\frac{\partial^2 T}{\partial x^2} + \frac{\partial^2 T}{\partial y^2} + \frac{\partial^2 T}{\partial Z^2}\right) - U\frac{\partial T}{\partial x} = 0 \qquad (6\text{-}9)$$

where α ($\equiv k/\rho C_p$) is the thermal diffusivity of the workpiece; and U,

the traveling speed of welding. This equation is subjected to the following three boundary conditions:

$$\left.\begin{aligned} &\frac{\partial T}{\partial Z} = 0 \text{ at } Z = 0 \text{ or } Z = W \\ &\lim_{r \to 0}\left(-2\pi r^2 W k \frac{\partial T}{\partial r}\right) = Q \end{aligned}\right\} \qquad (6\text{-}10)$$

$$T = T_0 \text{ as } r \to \infty$$

where $r = (x^2 + y^2 + Z^2)^{1/2}$ is the radial distance; W, the thickness of the segment; and T_0, the temperature of the workpiece before welding. General solution of Equation (6-9) subjected to boundary conditions (6-10) is a complicated summations of exponential functions. Tsai (1982) introduced a semi-empirical analytical solution with the consideration of simplification of general solution. The solution can be given by

$$T - T_0 = \frac{Q}{2\pi k r} \exp\left[- \left(\frac{ur}{2\alpha}\right)^2 \right] \qquad (6\text{-}11)$$

In order to estimate the crown and root widths, let us assume that the point source at upper half of the convective heat loss through the workpiece contritutues to the thermal melting process of crown width from solid to molten states, while the point source at lower half of that provides the thermal energy similarly for the melting process of root width. As we can observe from the facts that both the governing equation and boundary conditions are linear, solution of temperature distribution based on the contributions made by two point sources, point source at the upper half of workpiece and point source at the lower half of workpiece, shall be a superposition of the solutions

from these two point sources. This can be shown as

$$T - T_o = \frac{Q_1}{2\pi k r_1} \exp\left[- \left(\frac{ur}{2\alpha}\right)^2 \right] + \frac{Q_2}{2\pi k r_2} \cdot \exp\left[- \left(\frac{ur_2}{2\alpha}\right)^2 \right] \qquad (6\text{-}12)$$

where Q_1 and Q_2 denote heat source intensities of upper heat source and lower heat source, respectively. Here r_1 and r_2 stand for the radial distances from the point interests to upper heat source and lower heat source, respectively. Figure 8 shows the geometrical coordinate of this cross-sectional area of welding puddle. Let us consider to solve for crown width d_c width an assumption of temperature T to be melting temperature of metal T_m, we have

$$T_m - T_o = \frac{Q_1}{2\pi k(d_c/2)} \exp\left[- \left(\frac{U}{2\alpha} \cdot \frac{d_c}{2}\right)^2 \right] + \frac{Q_2}{2\pi k[(d_c/2)^2 + (W)^2]^{1/2}} \exp\left\{ - \left(\frac{U}{2\alpha}\right)^2 [(d_c/2)^2 + W^2] \right\} \qquad (6\text{-}13)$$

From Table 2, we have the upper half of the convective heat loss as

$$\sum_j (P_j)_u = 439 + 497 + 1/2(494) = 1183 \text{ W}$$

and the lower half of the convective heat loss as

$$\Sigma (P_j)_u = 1/2(494) + 350 + 211 = 808 \text{ W}$$

Also from Table 2, we have upper half and lower half heat transfer surface area of finger ring-shaped molten metal keyhole as

$$\sum_j (A_j)_u = \sum_j (A_j)_L = 0.14247 + 0.190 + 1/2(0.2256) = 0.44527 \text{ cm}^2$$

Upper half and lower half circumferential area of keyhole is

$$A_u = A_L = \pi DW/2$$

$$= \pi[(0.1562 \text{ in})(2.54 \text{ cm/in})][(0.375 \text{ in})(2.54 \text{ cm/in})/2]$$

$$= 0.5936 \text{ cm}^2$$

and

$$Q_1 = \frac{A_u}{\sum_j (A_j)_u} \sum_j (P_j)_u$$

$$= \frac{0.5936}{0.44527} (1183) = 1577.1 \text{ W}$$

and

$$Q_2 = \frac{A_L}{\sum_j (A_j)_L} \sum_j (P_j)_L$$

$$= \frac{0.5936}{0.44527} (808) = 1077 \text{ W}$$

In our case, workpiece material is AL #2219-T87, we have material constants and the grouping of physical parameters as follows:

$$\rho = 2.84 \times 10^3 \text{ kg/m}^3, \; C_p = 864 \text{ J/kg·K}, \; k = 130 \text{ W/m·}^0\text{K}$$

$$T_m = 916 \text{ K}, \; U = 8 \text{ in/min} = 3.387 \times 10^{-3} \text{ m/s}$$

$$\alpha = \frac{k}{\rho C_p} = \frac{130 \text{ W/m·}^0\text{K}}{(2.84 \times 10^3 \text{ kg/m}^3)(864 \text{ J/kg·K})} = 5.298 \times 10^{-5} \text{ m}^2/\text{s}$$

Substituting these values to Equation (6-13), one has

$$618 \text{ K} = \frac{(1577.1 \text{ W})}{\pi(130 \text{ W/m·k}) d_c} \exp\left(- \left[\frac{(3.387 \times 10^{-3} \text{ m/s}) d_c}{4(5.298 \times 10^{-5} \text{ m}^2/\text{s})} \right]^2 \right)$$

$$+ \frac{(1077 \text{ W})}{\pi(130 \text{ W/mk})[d_c^2 + (4)(9.525 \times 10^{-3} \text{ m})^2]^{1/2}}.$$

$$\cdot \exp\left(- \left[\frac{3.387 \times 10^{-3} \text{ m/s}}{(4)(5.298 \times 10^{-5} \text{m}^2/\text{s}} \right]^2 [d_c^2 + (4)(9.525 \times 10^{-3} \text{ m})^2] \right)$$

Solving for d_c, we have crown width as

$$d_c = 8.22 \times 10^{-3} \text{ m} = 8.22 \text{ mm}$$

Similarly, we have root width as

$$d_r = 6.58 \times 10^{-3} \text{ m} = 6.58 \text{ mm}$$

(E) Power Consumed in the Full Penetration of Workpiece

Most of the power absorbed by the workpiece in the welding is used in the melting of the workpiece. Assuming the puddle is and circular. The volume of puddle melted per unit of time is

$$\dot{V} = \frac{1}{3} \pi W \left[\left(\frac{d_c}{2}\right)^2 + \left(\frac{d_r}{2}\right)^2 + \left(\frac{d_c}{2}\right)\left(\frac{d_r}{2}\right) \right] + \frac{W}{2} (d_c + d_r) U$$

$$= \frac{\pi}{12} W (d_c^2 + d_r^2 + d_c d_r) + \frac{W}{2} (d_c + d_r) U$$

$$= \frac{\pi}{12} (9.525 \times 10^{-3} \text{ m})[(8.22 \times 10^{-3} \text{ m})^2 + (6.58 \times 10^{-3} \text{ m})^2$$

$$+ (8.22 \times 10^{-3} \text{ m})(6.58 \times 10^{-3} \text{ m})] + \frac{1}{2} (9.525 \times 10^{-3} \text{ m})$$

$$\cdot [(8.22 \times 10^{-3} \text{ m}) + (6.58 \times 10^{-3} \text{ m})](3.387 \times 10^{-3} \text{ m/s})$$

$$= 6.50 \times 10^{-7} \text{ m}^3/\text{s}$$

It is assumed that the puddle temperature is the melting temperature of the workpiece. The power absorbed by the workpiece for the full penetration of plasma arc is

$$\dot{Q} = \dot{\rho v H} + \dot{\rho v C_p (T_m - T_e)}$$

where H is the heat of fusion, and T_e is the environmental temperature of workpiece. In our case, the workpiece material is AL #2219-T87,

the corresponding material constants are as follows:

$$\rho = 2.84 \times 10^3 \text{ kg/m}^3, \quad H = 387 \times 10^3 \text{ J/kg},$$

$$C_p = 864 \text{ J/kg·K}, \quad T_e = 298 \text{ K}, \quad T_m = 916 \text{ K}$$

Thus, the power absorbed by the workpiece for full penetration of plasma arc is

$$\dot{Q} = \dot{\rho v}[H + C_p(T_m - T_e)]$$

$$= (2.84 \times 10^3 \text{ kg/m}^3)(6.50 \times 10^{-7} \text{ m}^3/\text{s})[(387 \times 10^3 \text{ J/kg}) + (864 \text{ J/kg·K})(916 - 298\text{k})]$$

$$= 1700 \text{ W}$$

From the flow parameters shown in Table 2 and the calculation of crown and root widths, the total absorption of power for plasma arc jet between the inlet and outlet ends of workpiece is 1991 W which shall be able to provide enough energy for the plasma arc jet to penetrate the workpiece completely. In this calculation, it shows that thermal power needed to melt workpiece is 1700 W. In other words, the thermal energy provided by the plasma arc jet which is absorbed by the workpiece is far greater than the energy needed to melt the material completely for penetrating through the workpiece.

Summary of flow zones including flow through nozzle, flow between the outlet of nozzle to the workpiece, and the flow through keyhole are illustrated in Table 3.

(VII) Calculation of Crown and Root Heights

Assuming the shape of the bead reinforcement is in the form of parabolic. The coordinate system is chosen to establish in crown bead. h_c and h_r are the crown and root heights, respectively. Figure 8 shows the adopted coordinate system for the mathematical

formulation.

The configuration of crown bead can be shown in the following equation:

$$Z = -\frac{4h_c}{d_c^2} y^2 + h_c$$

The cross-sectional area of crown reinforcement is

$$A_c = 2\int_0^{d_c/2}\left(-\frac{4h_c}{d_c^2} y^2 + h_c\right)dy = \frac{2}{3} h_c d_c$$

Similarly, the cross-sectional area of root reinforcement is

$$A_r = \frac{2}{3} h_r d_r$$

As the cross-sectional area of welding increment is provided by the wire feed, following relation is derived based on the conservation of metal volume and the gap of workpiece:

$$\frac{2}{3}d_c h_c + \frac{2}{3}d_r h_r = \frac{\pi}{4}d_w^2\frac{V_w}{U} - W\,W_g \qquad (7\text{-}1)$$

where d_w denotes wire feeder diameter; V_w, the wire feeding velocity; U, the traveling seed of welding; and W_g, the gap distance between two workpieces. Figure 9 shows the free body diagram and the geometry of the coordinate.

From the figure shown in Figure 9, the cross-sectional areas of a, b and c illustrated can be calculated separately as follows:

$$A_a = 2\int_0^{d_r/2}\left(-\frac{4h_c}{d_c^2}y^2 + h_c\right)dy = h_c d_r - \frac{1}{3} h_c d_c \left(\frac{d_r}{d_c}\right)^3$$

$$A_b = d_r W$$

$$A_c = \frac{2}{3} d_r h_r$$

The slopes at the points B and D are

$$\tan \alpha = \left. \frac{dz}{dy} \right|_{y=d_r/2} = - \frac{4h_c}{d_c} \left(\frac{d_r}{d_c} \right)$$

$$\tan \beta = \left. \frac{dz}{dy} \right|_{y=d_r/2} = - \frac{4h_r}{d_r}$$

From free-body diagram, shown in Figure 9, the equilibrium equation of forces gives

$$\left[h_c d_r - \frac{1}{3} h_c d_c \left(\frac{d_r}{d_c} \right)^3 + d_r W + \frac{2}{3} d_r h_r \right] \rho g$$

$$= 2 \left[\frac{4h_r}{d_r} - \frac{4h_c}{d_c} \left(\frac{d_r}{d_c} \right) \right] \sigma - \bar{P} d_r \qquad (7\text{-}2)$$

(A) Order Estimation of External Pressure Acting on the Crown

It is found from the experimental observation of the crown and root heights of welding that the effective external pressure acting on the surface of crown is in the pressure zone between the stagnation pressure of plasma arc jet and the hydrostatic pressure of shielding gas when the VPPA welding system was traveling through the crown during the process of material solidification. This assumption can be checked from the mathematical computation of the external pressure acting on the crown based on the profiles of crown and root measured from the experiment.

Experimental measurements of the profiles of crown and root, as shown in the Figure 8, are as follows:

d_c = 9 mm, d_r = 8 mm

h_c = 1.3 mm , h_r = 1.3 mm

and W = 6.35 mm for the material of AL #2219-T87 used for workpiece.

Rewriting equation (7-2), we have

$$\bar{P} = 8\left(\frac{h_r}{d_r^2} - \frac{h_c}{d_c^2}\right)\sigma - \left[h_c - \frac{1}{3}\left(\frac{d_r}{d_c}\right)^3 h_c + W + \frac{2}{3}h_r\right]\rho g \qquad (7\text{-}3)$$

Measurement of specimen is based on vertical welding condition. Under this conditon, direction of bead heights and the direction of gravitational force are mutually perpendicular. This makes that the contribution of gravitational force is not effective on the determination of bead heights. With neglecting gravitational force, Equation (7-3) becomes

$$\bar{P} = 8\left(\frac{h_r}{d_r^2} - \frac{h_c}{d_c^2}\right)\sigma \qquad (7\text{-}4)$$

This equation is true only for puddle in a molten state while the experimental measurement is made after the solidification of puddle. Shrinkage of crown height will be resulted in a phase transition from molten metal to solidified metal. Detailed consideration of the metal shrinkage during the solidification process will be discussed in Section VII-C of this report. Results from Section VII-C, shown in Equation (7-15), will be used in this study for the modification of crown height, h_c, after the phase transition from molten metal to solidified metal. From Equation (7-15), shrinkage of crown height is

$$\Delta h_c' = \frac{3}{4} W \frac{\Delta V}{V} = \frac{3}{4}(6.35)(0.067) = 0.32 \text{ mm}$$

Here, W stands the thickness of workpiece; and $\Delta V/V$, the specific volumetric shrinkage. King (1987) shows that the specific volumetric shrinkage for Aluminum during the solidification process is 6.7%. Thus, the crown height before the solidification process is given by

$$h_c' = h_c + \Delta h_c' = 1.3 + 0.32 = 1.62 \text{ mm}$$

Now contribution from root surface tension pressure is

$$P_{sr} = 8\frac{h_r}{d_r^2}\sigma = (8)\frac{1.3 \times 10^{-3} \text{ m}}{(8 \times 10^{-3} \text{ m})_2}(0.865 \text{ N/m}) \quad (7\text{-}5)$$

$$= 140.56 \text{ p}_a$$

Contribution from crown surface tension pressure is

$$P_{sc} = \frac{h_c'}{d_c^2}\sigma = (8)\frac{1.62 \times 10^{-3} \text{ m}}{(9 \times 10^{-3} \text{ m})^2}(0.865 \text{ N/m}) \quad (7\text{-}6)$$

$$= 138.40 \text{ P}_a$$

Thus, the external pressure acting on the crown is

$$\bar{P} = P_{sr} - P_{sc}$$

$$= 140.56 - 138.40 = 2.16 \text{ P}_a$$

In other words, the external pressure acting on the crown is

$$\frac{\bar{P}}{P_{sr}} = \frac{2.16}{140.50} = 1.5\%$$

of the root surface tension pressure, and is

$$\frac{\bar{P}}{P_{sc}} = \frac{2.16}{138.4} = 1.5\%$$

of the crown surface tension pressure. Based on this estimation, it is shown that the external pressure acting on the crown is less than 1.5% of the either crown surface tension pressure or root surface

tension pressure. Thus, it can be ignored from the crown and root heights calculation.

(B) Crown Height and Root Height Under Normal Gravity

Rewrite Equation (7-2) with neglecting the pressure term,

$$\left[d_r - \frac{1}{3} d_c \left(\frac{d_r}{d_c}\right)^3 + \frac{8}{d_c}\left(\frac{d_r}{d_c}\right)\frac{\sigma}{\rho g} \right] h_c + \left[\frac{2}{3} d_r - \frac{8}{d_r}\frac{\sigma}{\rho g} \right] h_r = - d_r W \qquad (7\text{-}7)$$

Solving for h_c from Equations (7-1) and (7-3), we have

$$h_c = \frac{-\left(1 - \frac{12}{d_r^2}\frac{\sigma}{\rho g}\right)\left(\frac{\pi}{4} d_w^2 \frac{V_w}{U} - W W_g\right) - d_r W}{d_r - \frac{2}{3} d_c + \frac{8\sigma}{\rho g}\left[\frac{1}{d_c}\left(\frac{d_r}{d_c}\right) + \frac{d_c}{d_r^2}\right] - \frac{1}{3} d_c \left(\frac{d_r}{d_c}\right)^3} \qquad (7\text{-}8)$$

In our case of VPPA welding system operated at NASA/MSFC, following values of physical parameters are adopted: σ = 0.865 N/m, g = 9.81 m/s^2, V_w = 38 in/min, U = 8 in/min, W = 9.525 x 10^{-3} m, and W_g = 3.387 x 10^{-5} m. Aluminum density at 25^{0}C, ρ = 2.84 x 10^3 kg/m^3. Aluminum density at molten state before the solidification can be calculated by taking specific volumetric shrinkage into consideration, $\rho' = \rho(1 - \Delta V/V)$ = 2.84 x 10^{-3}(1-0.067) = 2.65 x 10^3 kg/m^3.

$$\frac{\sigma}{\rho g} = \frac{0.865 \text{ N/m}}{(2.65 \times 10^3 \text{ kg/m}^3)(9.81 \text{ m/s}^2)} = 3.33 \times 10^{-5} \text{ m}^2$$

$$\frac{\pi}{4} d_w^2 \frac{V_w}{U} = \left[\frac{\pi}{4}\left(\frac{1}{16} \times 0.0254 \text{ m}\right)^2\right] \frac{(38 \text{ in/min})}{(8 \text{ in/min})} = 9.402 \times 10^{-6} \text{ m}^2$$

$$\frac{d_r}{d_c} = \frac{6.58 \text{ mm}}{8.22 \text{ mm}} = 0.8; \quad d_c\left(\frac{d_r}{d_c}\right)^3 = (8.22 \times 10^{-3} \text{ m})(0.8)^3$$

$$= 4.216 \times 10^{-3} \text{ m}$$

Thus, we can determine the crown height by substituting the values of above mentioned parameters in Equation(7-8)

$$h_c = \left\{ - \left[1 - \frac{(12)(3.33 \times 10^{-5} \text{ m}^2)}{(6.58 \times 10^{-3})^2} \right] [9.402 \times 10^{-6} \text{ m}^2 - (9.525 \times 10^{-3} \text{ m})(3.38 \times 10^{-5} \text{ m})] - (6.58 \times 10^{-3} \text{ m}) \cdot \cdot (9.525 \times 10^{-3} \text{ m}) \right\} \Big/ \left\{ (6.58 \times 10^{-3} \text{ m}) - \left(\frac{2}{3} \times 8.22 \times 10^{-3} \text{ m} \right) + (8)(3.33 \times 10^{-5} \text{ m}^2) \cdot \left[\frac{0.8}{8.22 \times 10^{-3} \text{ m}} + \frac{8.22 \times 10^{-3} \text{ m}}{(6.58 \times 10^{-3} \text{ m})^2} \right] - \frac{1}{3} (4.216 \times 10^{-3} \text{ m}) \right\} = 0.16 \text{ mm}$$

Similarly, we have the root height

$$h_r = 1.87 \text{ mm}$$

$$\text{Thus, for Crown Bead} \begin{cases} \text{Width: } 8.22 \text{ mm} \\ \text{Height: } 0.16 \text{ mm} \end{cases} \quad \text{for Root Bead} \begin{cases} \text{Width: } 6.58 \text{ mm} \\ \text{Height: } 1.87 \text{ mm} \end{cases} \qquad (7\text{-}9)$$

under normal gravity conditions.

(C) Crown and Root Heights Under Vertical Welding Condition

Under vertical welding condition, direction of bead heights and direction of gravitational force are mutually perpendicular. This makes the contribution aof gravitational force on the determination of bead heights ineffective. Let us consider Equation

(7-2) with neglecting P and g for vertical welding condition. Following equation is obtained:

$$\frac{h_r}{d_r^2}\,\sigma_r = \frac{h_c}{d_c^2}\,\sigma_c \qquad (7\text{-}10)$$

Based on Robert and Melvin (1981) for the material of AL #2219, we have relation for surface tension coefficient as the function of temperature distribution,

$$\sigma = 865 - 0.14(T - T_m) \text{ dyne/cm} \qquad (7\text{-}11)$$

where T_m denotes the melting temperature of the material.

Assuming that root surface temperature is same as the temperature of crown surface, Equation (7-10) can be simplified to

$$h_r = h_c\left(\frac{d_r}{d_c}\right)^2 \qquad (7\text{-}12)$$

One can solve Equations (7-1) and (7-12) simultaneously with substitution of following data based on VPPA welding system operated at NASA/MSFC: d_w = 1/16 in, U = 8 in/min, V_w = 38 in/min, $W_g = 3.387 \times 10^{-5}$ m, d_c = 8.22 mm, and d_r = 6.58 mm. It leads

$$h_c = 1.09 \text{ mm}$$

and

$$h_r = 0.70 \text{ mm}$$

These crown and root heights stand for heights of crown and root at the stage of molten metal state. There is a phase transition from liquid to solid during the metal solidification which accompanies with shrinkage of volume.

Figure 10(A) shows the configuration of the cross-section of puddle with the interface between liquid (molten metal) and solid metal. As the temperature start to drop down, solidification of

metal is observed at the interface between the molten and solid metals of the workpiece. Figure 10(B) shows the configuration of puddle with a trapezoid-shaped liquid-solid interface which moves gradually toward the center due to the solidification of metal. It shows that the solidified metal is accumulated toward the root side because root temperature is lower than the crown temperature which makes the solidification faster in the root side than the crown side. Figure 10(C) shows the configuration of the cross-section of puddle during the process of solidification. This figure shows that the shrinkage of crown height is observed during the process of metal solidification. Cross-sectional area of puddle with molten metal can be approximated as

$$A \simeq \frac{1}{2} W d_c'$$

where W stands the thickness of workpiece; and d_c', the crown width in a state of molten metal. Let us choose specific volumetric shrinkage, $\Delta v/v$, to be a parameter of material property during a metalic solidification process, variation of cross-sectional area of puddle can be shown in the following relation:

$$\Delta A = A\left(\frac{\Delta v}{v}\right) = \frac{1}{2} W d_c' \left(\frac{\Delta v}{v}\right) \qquad (7\text{-}13)$$

It is shown in Equation (7-1) for the cross-sectional area of root reinforcement as

$$\Delta A = \Delta\left(\frac{2}{3} d_c' h'\right) = \frac{2}{3} d_c' \, \Delta h' \qquad (7\text{-}14)$$

From Equations (7-13) and (7-14), it leads

$$\frac{1}{2} W d_c' \left(\frac{\Delta v}{v}\right) = \frac{2}{3} d_c' \Delta h'$$

Thus,

$$\Delta h' = \frac{3}{4} W \frac{\Delta v}{v} \qquad (7\text{-}15)$$

Based on King (1987), specific volumetric shrinkage for Aluminum during the solidification process is 6.7%. Therefore, we have the crown height shrinkage

$$\Delta h' = \left(\frac{3}{4}\right)(9.525 \text{ mm})(0.067) = 0.48 \text{ mm}$$

This calculation implies that the final crown height after the metalic solidification becomes 1.09 - 0.48 = 0.61 mm. Thus, we have

$$\left.\begin{array}{l} \text{crown} \begin{cases} \text{width} = 8.22 \text{ mm} \\ \text{height} = 0.61 \text{ mm} \end{cases} \\ \text{root} \begin{cases} \text{width} = 6.58 \text{ mm} \\ \text{height} = 0.70 \text{ mm} \end{cases} \end{array}\right\} \qquad (7\text{-}16)$$

This result shows that root height is greater than crown height even for the case that we neglect the contribution of gravitational force for the vertical welding if we take the shrinkage effect during the metal solidification into consideration.

VIII. Discussion and Conclusion

Flow profile and power distribution of argon plasma gas as a working fluid in the VPPA welding process has been analyzed. The purpose of this study is to provide a suitable algorithm for computation simulation of the flow field, energy distribution and the prediction of the final production of welding in terms of crown and

for flow of plasma jet between outlet of nozzle to workpiece is 20%; and for flow through keyhole of workpiece is 23% with partial penetration, and 28.5% with full penetration. Majority of power absorbed by the keyhole of workpiece is used for melting the solid metal workpiece to become molten metalic puddle.

For the heat transfer effect on the workpiece, recent study imdicates that heat transfer rate out of the rear half of a keyhole is less than that of the front half. This implies that more heat transfer area is required for the front half than that of the rear half. In fact, the shape of keyhole with which plasma gas actually contact and transfer heat energy is like a finger ring.

Penetration depth of keyhole due to argon plasma jet has been calculated based on hydrodynamic balance of stagnation pressure of plasma jet, surface tension and hydrostatic head, and also the amount of thermal power absorbed by the workpiece to be used for melting keyhole with the power provided by the arc plasma jet. It shows that current VPPA welding system operated by the NASA/MSFC is capable to make full penetration for workpiece with a thickness of 0.375 in.

Crown and root widths, and corwn and root heights have been calculated. Crown and root widths are the function of thermal diffusivity, traveling speed of wilding, and melting temperature of metal. Crown and root heights are the function of wire feeder diameter, wire feeding velocity, traveling speed of welding, gap distance between two workpiece, crown and root widths, and the method of welding , such as vertical or horizontal welding. Configuration of crown and root reinforcement is the equilibrium of surface tension

pressure, gravitaitonal pressure and external pressure acting on the crown. Experimental measurement based on the welding speciment received shows that the order of external pressure and gravitational pressure acting on the crown is much smaller than that of surface tension pressure and gravitational pressure effective to the configuration of crown and root reinforcement. Root height is always greater than crown height for the case of horizontal welding under normal gravity condition. For the case of vertical welding condition in which the gravitational force is ineffective on the determination of bead heights, it shows that crown height is greater than root height when the puddle was in molten state before the phase transition from liquid (molten) to solidified metal. Solidification of metal starts at the interface between molten and solid metals of workpiece. It shows that the solidified metal is accumulated toward the root side because root temperature is lower than the crown termperature which makes the solidification faster in the root side than in the crown side. The volumetric shrinkage, during the phase transition from liquid to solid, makes the final figure of root height greater than that of crown height after the metal solidificaton.

Present research provides an algorithm for promoting automatic control of flow parameters and the dimensions of final product of welding specification to be used for the VPPA welding system operated at NASA/MSFC. This algorithm is essential for the automation of VPPA welding system, in particular for the operation of effective welding in a hostile environment such as Space Station at low Earth orbit. With the regulation of power input, such as pilot and main arc currents

and voltages for straight and reverse polarities, volumetric flow rates of argon gas for working fluid and helium gas for shielding gas, traveling speed of welding, wire feeder diameter, wire feeding velocity, traveling speed of welding, etc., one can very well modify the end product of welding through the computation of algorithm provided in this study.

Acknowledgement

The authors would like to express their gratitude to Dr. Arthur C. Nunes of Materials and Processes Laboratory, NASA Marshall Space Flight Center for stimulative discussions during the course of the present study. The authors also acknowledge the support of present work through the NASA Contract NAS8-36955/Delivery Order No. 37.

References

Abramovich, G. N., "The Theory of Turbulent Jets", PP. 671, MIT Press, MA., 1963.

American Society for Metals Handbook Committee, "Metals Handbook," 9th Edition, Vol. 2, PP. 855, American Society for Metals, Metals Park, OH, 1979.

Drellishak, K. S., Knopp, C. F., and Cambel, A. B., "Partition Function and Thermodynamic Properties of Argon Plasma," AEDC-TDR-63-146, PP. 238, Arnold Engineering Development Center, TN, 1963.

Hsu, Y. T., and Rubinsky, B., "Transient Melting of a Metal Plate by a Penetrating Plasma Arc," J. Heat Transfer, 109, 463-469, 1987.

Ibele, W., "Modern Developments in Heat Transfer", PP. 443, Academic Press, New York, 1963.

King, F., "Aluminum and Its Alloys", pp. 313, The Camelot Press, Southampton, United Kingdon, 1987.

Lancaster, J. F., "The Physics of Welding", 2nd Edition, PP. 340, Pergamon Press, Oxford, England, 1986.

Metcalfe, J. C., and Quigley, A. B. C., "Heat Transfer in Plasma Arc Welding", Welding Journal, 54, 995-1035, 1975.

Miller, H. R., and Filipski, S. P., "Automated Plasma Arc Welding for Aerospace and Cyogenic Fabrication", Welding Journal, 45, 493-501, 1966.

Nunes, A. C., Jr., Novak, H. L. and McIlwain, M. C., "Weld Geometry Strength Effect in 2219-T87 Aluminum", NASA Technical Memorandum TM-82404, 1981.

Nunes, A. C., Jr., Bayless, O. E., Jr., Jones, C. S., III, Munafo, P. M., Biddle, A. P., and Wilson, W. A., "The Variable Polarity Plasma Arc Welding Process: Its Application to the Space Shuttle External Tank-First Interim Report", NASA Technical Memorandum TM-82532, 1983.

Nunes, A. C., Jr., Bayless, O. E., Jr., Jones, C. S., III, Munafo, P. M., Biddle, A. P., and Wilson, W. A., "Variable Polarity Plasma Arc Welding on the Space Shuttle External Tank", Welding Journal, 63, 27-35, 1984a.

Nunes, A. C., Jr., Bayless, O. E., Jr., Jones, C. S., III, Munafo, P. M., Biddle, A. P., and Wilson, W. A., "Variable Polarity Plasma Arc Welding Process: Its Application to the Space Shuttle External Tank-Second Interim Report", NASA Technical Memorandum TM-86482, 1984b.

O'Brien, R. L., "Arc Plasma for Joining, Cutting and Surfacing", Welding Research Council, No. 131, 1968.

Privozhik, L. J., and Miller, H. R., "Evaluation of Plasma Arc Welding for 120 inch Diameter Rocket Motor Cases", Welding Journal, 45, 717-725, 1966.

Robert, C. W., and Melvin, J. A., "CRC Handbook of Chemistry and Physics", 61st Edition, CRC Press, NY, 1981.

Rosenthal, D., Welding Journal, 20, 220, 1941.

Tsai, C. L., "Modeling of Thermal Behaviors of Metal During Welding", in Trends in Welding Research in the United States, Edited by S. A. David, Amierican Society for Metals, pp. 91-108, 1982.

Figure Captions

Figure 1. VPPA electric power system. Left hand side shows the straight polarity mode, and the reverse polarity mode is shown on the right hand side.

Figure 2. Electric power input system and the dimension of the geometry for VPPA welding process.

Figure 3. Plasma arc power distribution in the whole VPPA welding system.

Figure 4. Electric current and voltage drop distribution of the VPPA welding system.

Figure 5. Impingement of plasma arc jet on the surface of weld pool.

Figure 6. Ring-shaped geometry of simplified heat transfer area of keyhole and it dimensions.

Figure 7. Moving coordinate system for three dimensional heat flow. X-coordinate is along welding traveling direction; Y-coordinate transverse to traveling direction; and Z-coordinate along the keyhole direction. Welding traveling speed is - U.

Figure 8. Geometrical coordinate of the cross-sectional area of welding puddle.

Figure 9. Free body diagram and the geometry of coordinate to describe the balance of forces among external pressure P, surface tension force, σ, and gravitational force g.

Figure 10. Configuration of the cross-section of puddle with the liquid (molten metal)-solid metal. (A) Molten state

puddle before phase transition, (B) Molten state puddle in the process of phase transition from molten state metal to solidified state metal; and (C) solidified metal of welding puddle.

Table 1: Power Loss Between Plasma. from Outlet End of Nozzle to Plasma at the Inlet End of the Keyhole of Workpiece

Segment	Entrance Temperature (°K)	Assumed Outlet Temperature (°K)	Average Temperature (°K)	Radiative Loss $\dot{Q}_R$ (W)	Convective Heat Loss $\dot{Q}_c$ (W)	Total Loss $\dot{Q}_R + \dot{Q}_c = P_t^L$ (W)	Oulet Power P_t (W)	Oulet Enthalpy (cal/g)	Computed Outlet Temperature (°K)
1	8760	10350	9555	147.61	15.51	163.12	648.28	1616.5	10370
2	10370	10830	10600	224.4	32.11	256.51	748.24	1865.7	10850
3	10850	11050	10950	255.12	40.62	295.74	808.97	2017.17	11070
4	11070	11230	11150	274.28	46.26	320.54	844.9	2106.75	11220
5	11220	11300	11260	285.26	49.61	334.87	866.5	2161.0	11300
Total				1186.67	184.11	1371			

Table 2 Convective Heat Loss Through Workpiece

Segment	Surface Area (cm^2)	Entrance Enthalpy $H_{j,i}$ (MJ/kg)	Assumed Outlet Enthalpy $H_{j,o}$ (MJ/kg)	Mean Enthalpy $\bar{H}_j$ (MJ/kg)	Convective Heat Transfer Loss P_j (W)	Heat Loss corresponding to Enthalpy difference between Inlet End and Outlet End of Segment $\dot{m}(H_{j,i} - H_{j,o})$ (W)
1	0.14247	28.716	24.1255	26.421	439	440
2	0.190	24.1255	18.93	21.53	497	498
3	0.2256	18.93	13.77	16.35	494	495
4	0.190	13.77	10.114	11.94	350	350
5	0.14247	10.144	7.923	9.019	211	210
Total					1991	1993

Table 3 Flow Zone Characteristics

Flow Zone	Flow Through Nozzle	Flow Between Outlet of Nozzle to Workpiece	Flow Through Keyhole
Average Temperature	10,680 °K	10,720 °K	12,575 °K
Reynold's Number	107.6	139.4 *	165.7
Prandtl's Number	0.76	0.604	0.36
Major Loss of Heat Transfer	Convective Heat Transfer	Radiative Heat Transfer	Convective Heat Transfer
Percentage of Power Loss	29.6%	20%	Partial Penetration 23% Full Penetration 28.5%
Flow Characteristics	Laminar Subsonic Flow	Turbulent Subsonic Flow *	Laminar Subsonic Flow
Entrance Temperature	12,600 °K	8,760 °K	14,280 °K
Outlet Temperature	8,760 °K	11,260 °K	10,870 °K
Boundary Layer Thickness Comparison	Thickness (Momentum Boundary Layer) > Thickness (Thermal Boundary Layer)	Thickness (Momentum Boundary Layer) > Thickness (Thermal Boundary Layer)	Thickness (Momentum Boundary Layer) > Thickness (Thermal Boundary Layer)

* Flow becomes Turbulence for free stream jet with ReNo. exceeding 100.

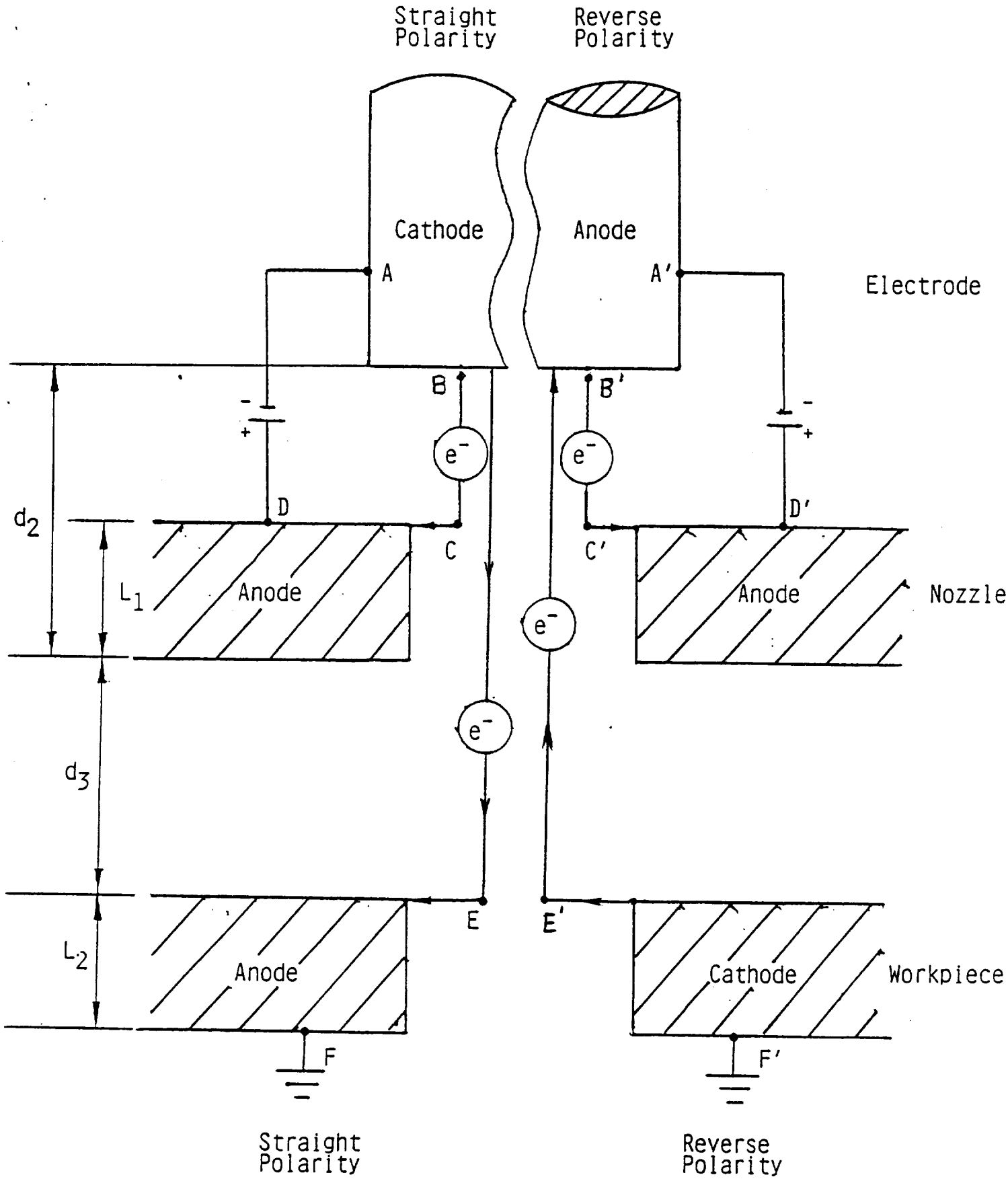
Straight Polarity
Reverse Polarity
Cathode
Anode
A
A'
Electrode
B
B'
e⁻
D
D'
C
C'
d2
L1
Anode
Anode
Nozzle
d3
E
E'
L2
Anode
Cathode
Workpiece
F
F'
Straight Polarity
Reverse Polarity

Fig. 1

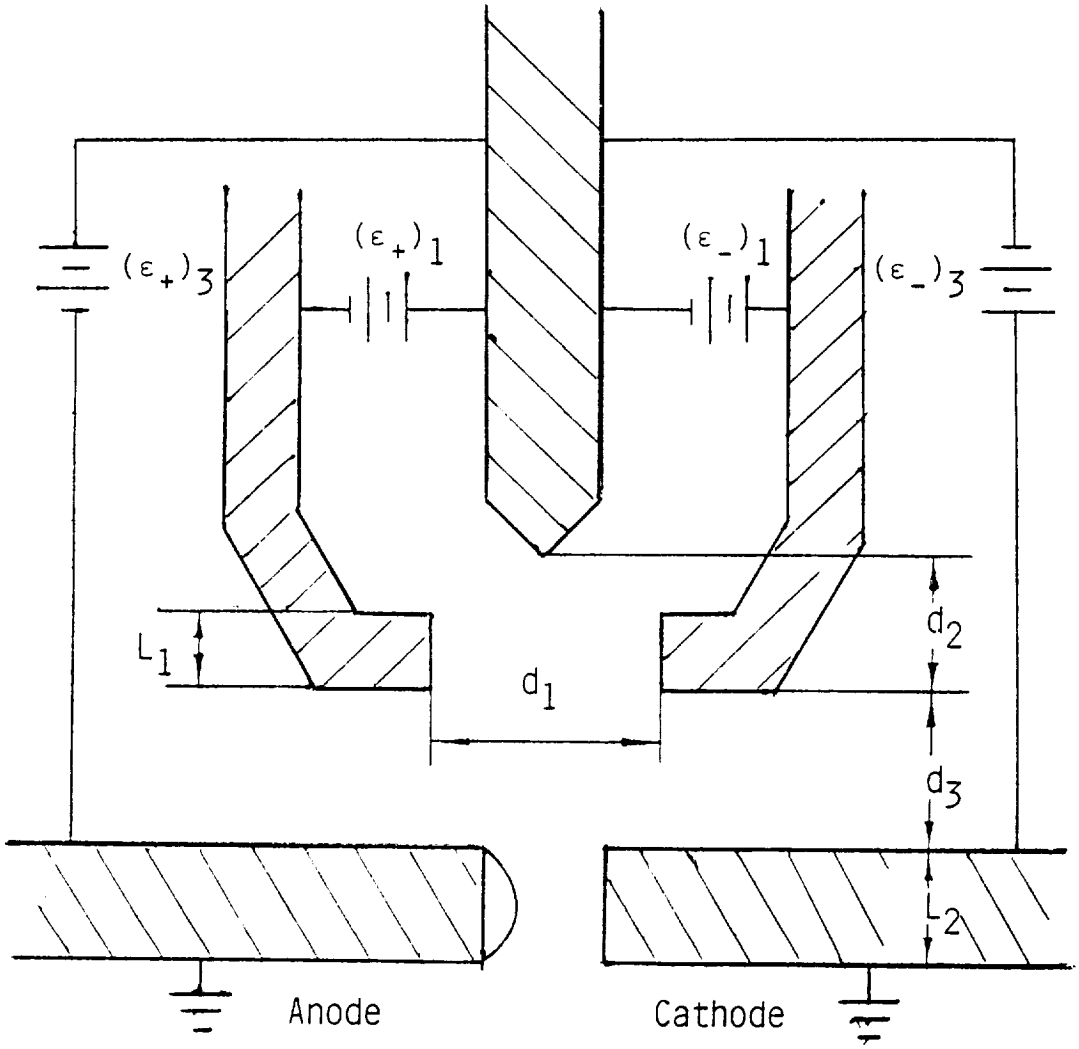

$d_1 = 0.1562$ in
$d_2 = 0.1780$ in
$d_3 = 0.2200$ in

$L_1 = 0.133$ in
$L_2 = 0.375$ in

Fig. 2

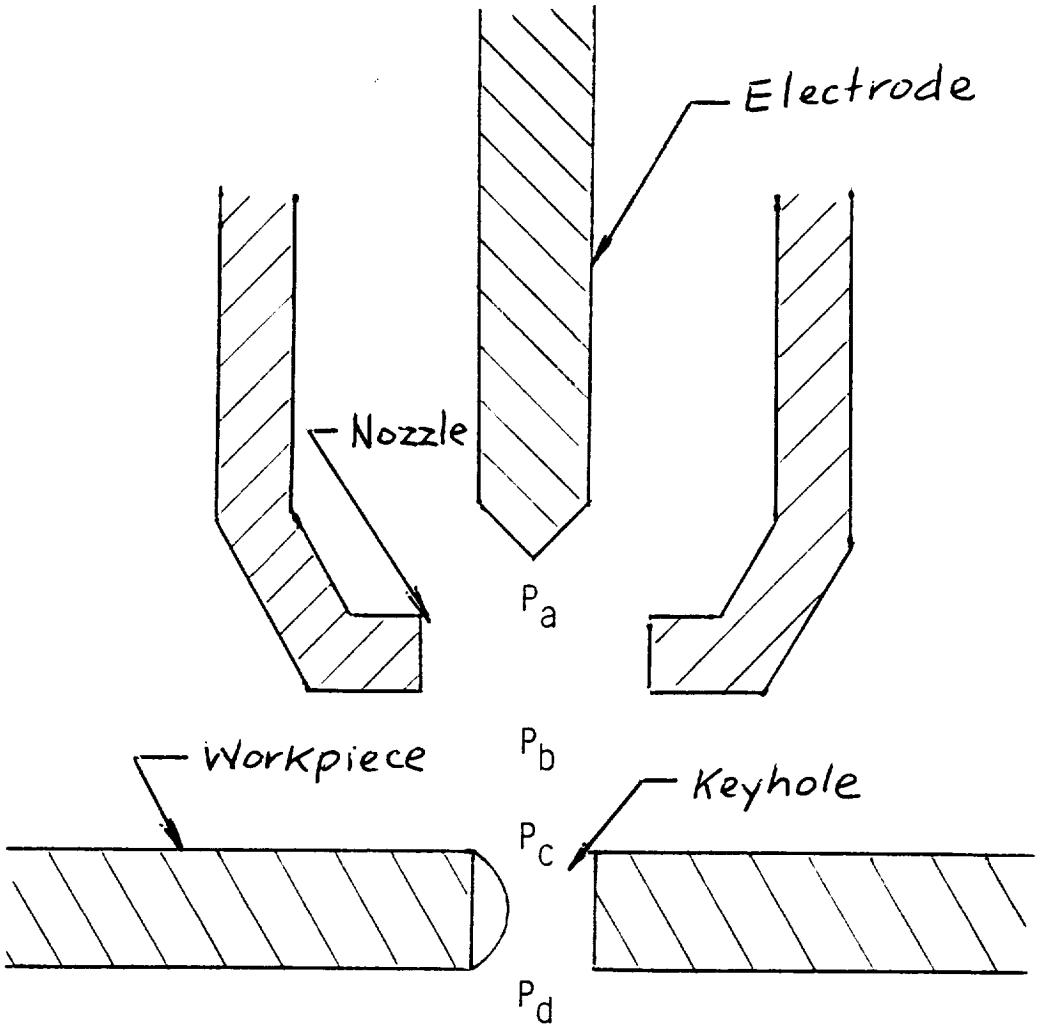

Fig. 3

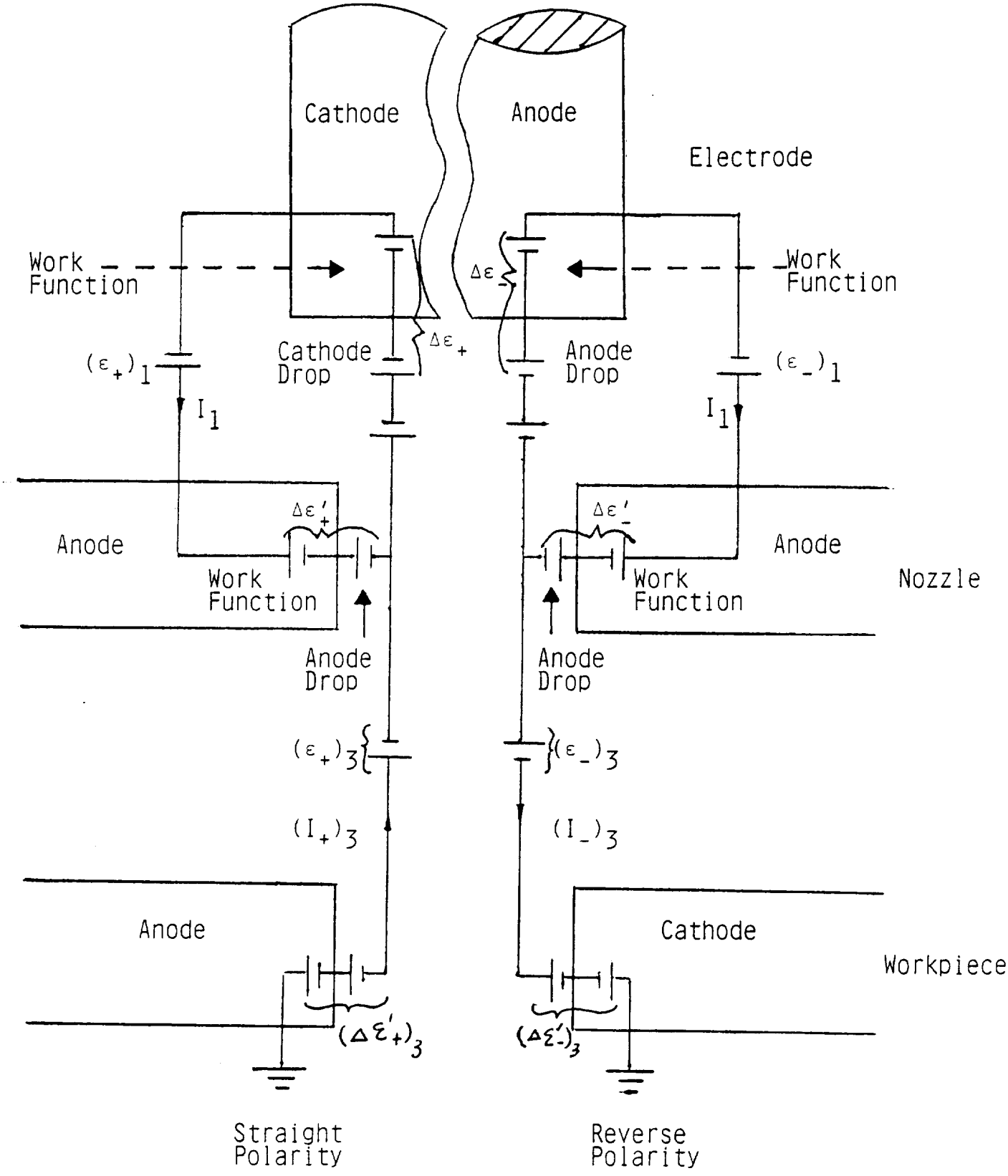
Cathode
Anode
Electrode
Work Function
Work Function
$\Delta\varepsilon_-$
$\Delta\varepsilon_+$
Cathode Drop
Anode Drop
$(\varepsilon_+)_1$
$(\varepsilon_-)_1$
I_1
I_1
$\Delta\varepsilon'_+$
$\Delta\varepsilon'_-$
Anode
Work Function
Anode
Work Function
Nozzle
Anode Drop
Anode Drop
$(\varepsilon_+)_3$
$(\varepsilon_-)_3$
$(I_+)_3$
$(I_-)_3$
Anode
Cathode
Workpiece
$(\Delta\varepsilon'_+)_3$
$(\Delta\varepsilon'_-)_3$
Straight Polarity
Reverse Polarity

Fig. 4

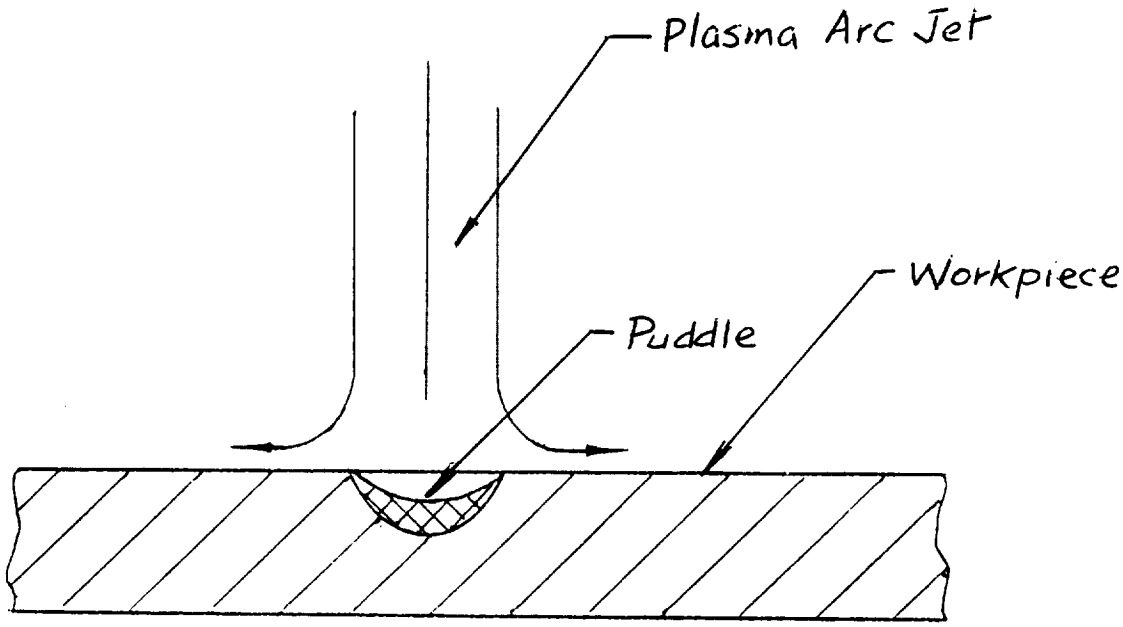

Fig. 5

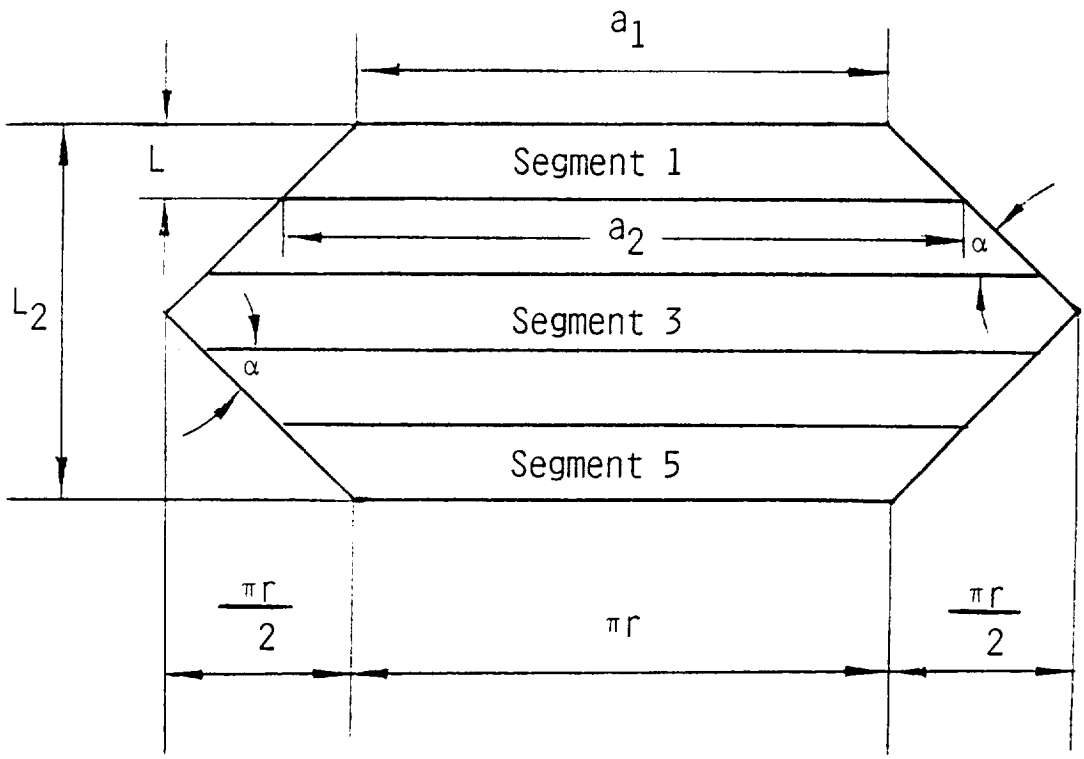

$$L = \frac{L_2}{5}$$

Fig. 6

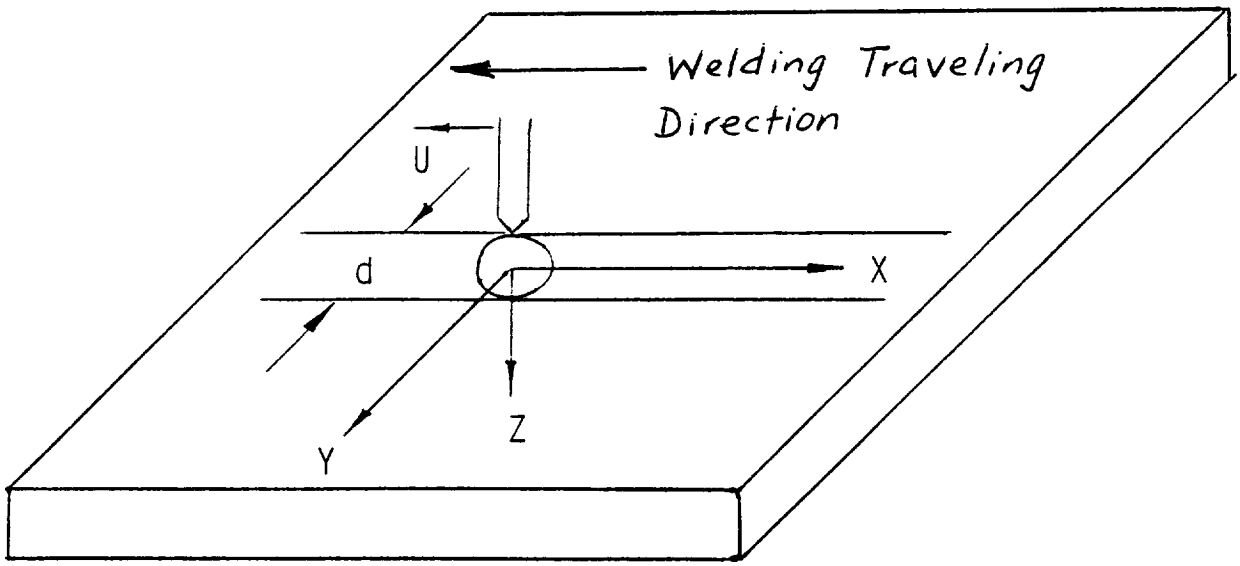

Fig. 7

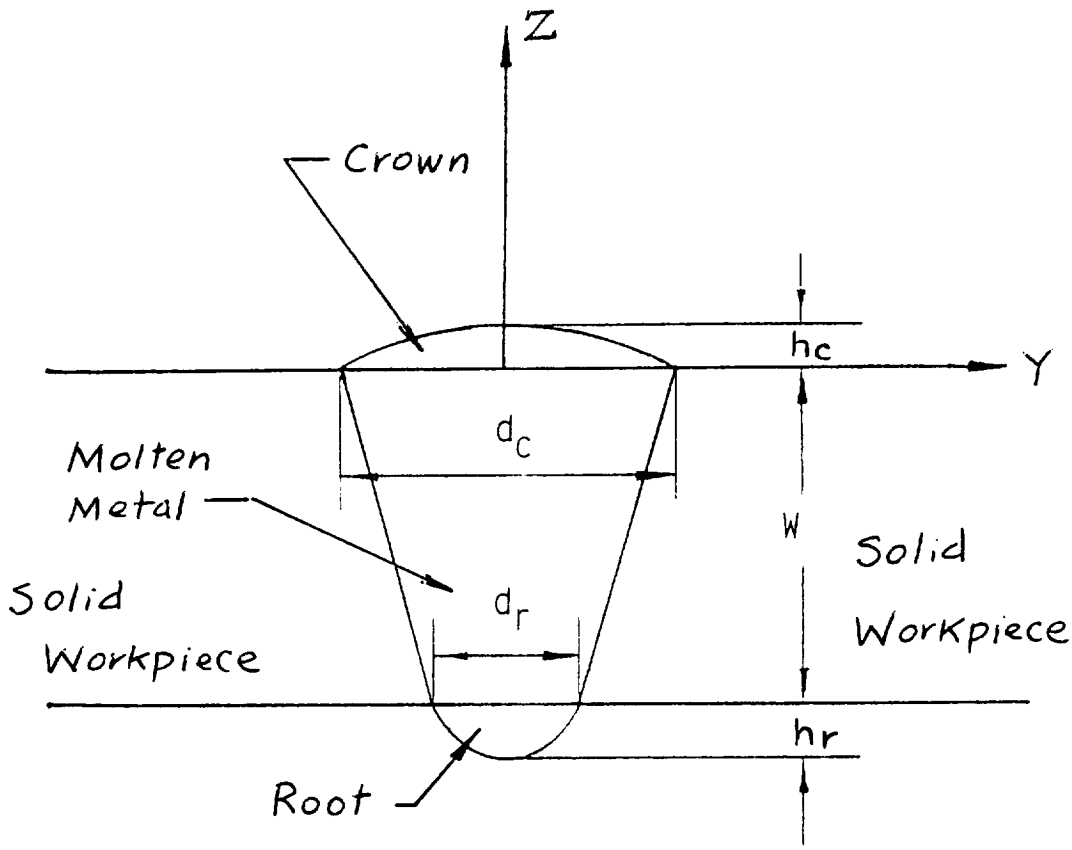
Z
Crown
hc
Y
dc
Molten
Metal
W
Solid
Workpiece
dr
Solid
Workpiece
hr
Root

Fig. 8

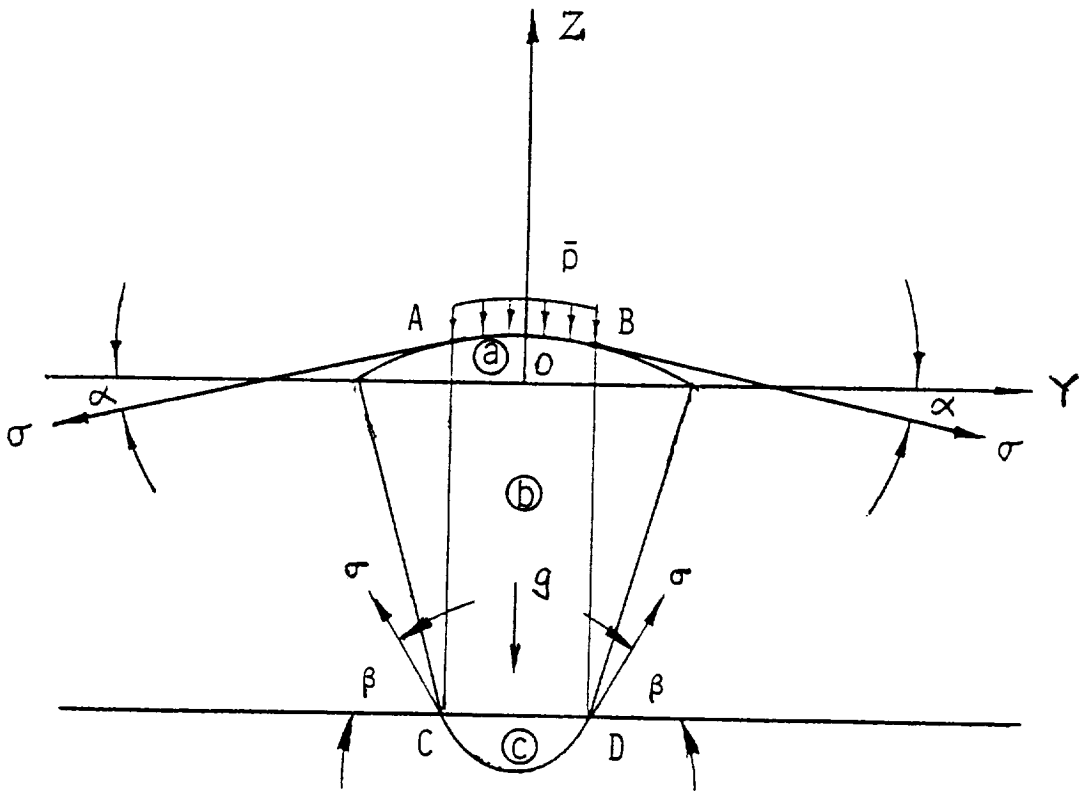

Fig. 9

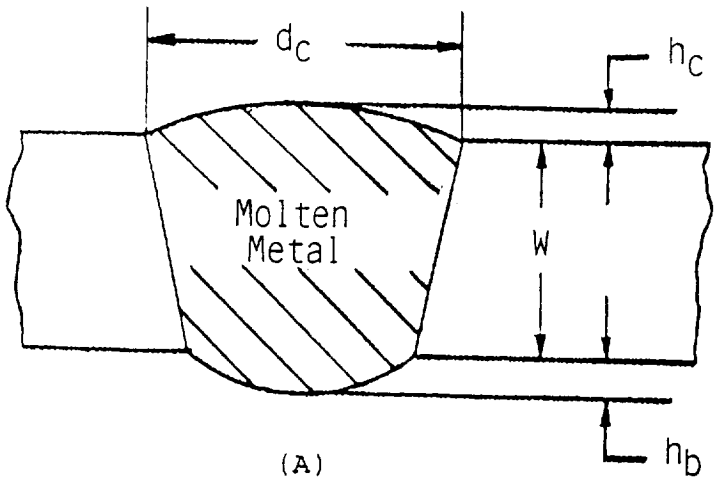

(A)

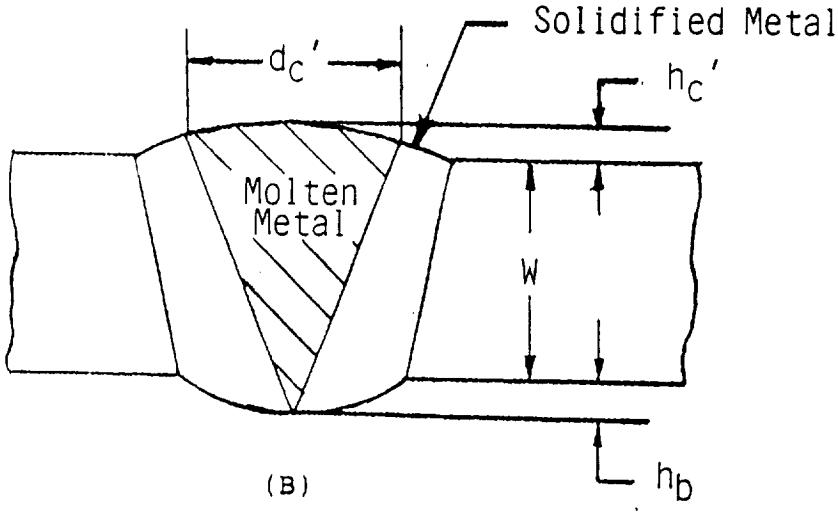

(B)

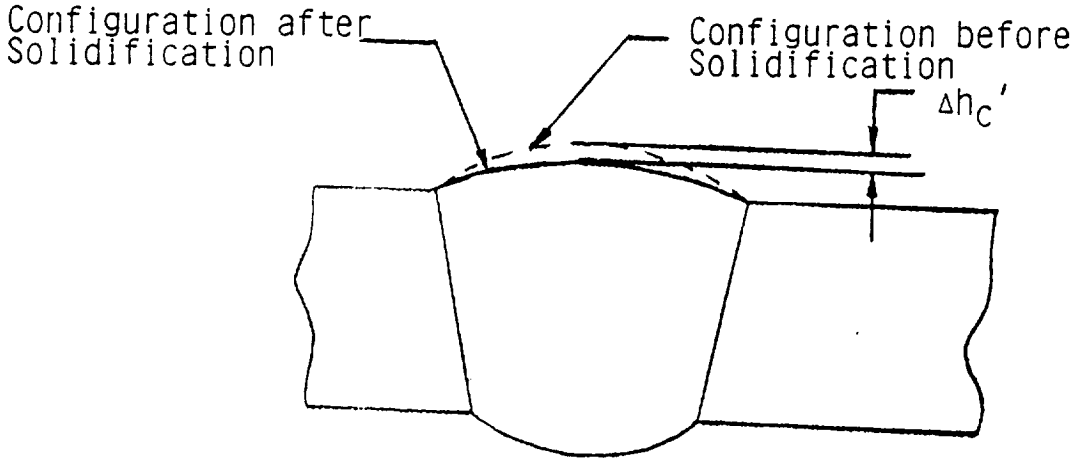

(C)

Figure 10 (A, B, C)